ON FERMIONIC CORRELATIONS IN HIGH-TEMPERATURE SUPERCONDUCTORS AND MOLECULAR SYSTEMS

F.L.J. VOS

ON FERMIONIC CORRELATIONS IN HIGH-TEMPERATURE SUPERCONDUCTORS AND MOLECULAR SYSTEMS

ON FERMIONIC CORRELATIONS IN HIGH-TEMPERATURE SUPERCONDUCTORS AND MOLECULAR SYSTEMS

PROEFSCHRIFT

TER VERKRIJGING VAN DE GRAAD VAN DOCTOR
AAN DE RIJKSUNIVERSITEIT TE LEIDEN,
OP GEZAG VAN DE RECTOR MAGNIFICUS DR. W. A. WAGENAAR,
HOOGLERAAR IN DE FACULTEIT DER SOCIALE WETENSCHAPPEN,
VOLGENS BESLUIT VAN HET COLLEGE VOOR PROMOTIES
TE VERDEDIGEN OP DONDERDAG 2 APRIL 1998
TE KLOKKE 14.15 UUR

DOOR

Fernando Leonard Jacobus Vos

geboren te Amsterdam op 18 maart 1965

Promotiecommissie:

Promotor:	prof. dr. ir. W. van Saarloos
Referent:	dr. J. Zaanen
Overige leden:	prof. dr. D. P. Aalberts
	prof. dr. P. J. van Baal
	prof. dr. C. W. J. Beenakker
	dr. H. J. M. de Groot
	prof. dr. L. J. de Jongh
	prof. dr. J. M. J. van Leeuwen

Voor Monique, Danielle,
mijn schoonouders en
mijn moeder.

Contents

1 Introduction

In spite of the strong interactions that electrons have through the Coulomb potential, the developments in solid state physics over the last sixty years have shown that quite often the electron-electron interactions can be neglected to a very good approximation. One of the most vivid technologically relevant illustrations of this comes from the semiconductor industry — the transport of electrons and holes in the semiconductor materials from which microchips are usually made, is normally described entirely in terms of a one-electron picture. This means that, instead of taking the correlations between the fermions (electrons) into account, one can limit the analysis to that of a single electron in an effective periodic potential — a Bloch-electron. This effective potential may itself incorporate the effects of the interactions with the other electrons in some average way [1].

Such a description is not only successful for semiconductors, but also for many of the classical metals. In this case, the theoretical justification for describing transport and other properties in terms of almost non-interacting quasiparticles, is the Landau Fermi-Liquid theory [1,2]. In the last two decades, more and more examples have been found of materials or of artificially structured devices, for which such a simple description fails. Notable examples include new materials like heavy fermions, Kondo materials, high-temperature superconductors and the recently discovered materials with a "giant" or "colossal" magnetoresistance. Also, surprising and fundamentally new manifestations of interaction effects have been found in suitably engineered structures of materials whose bulk behavior itself is classical. For example, in layered materials one can create quasi-two-dimensional electron gases. In the early eighties, new quantum Hall effects were discovered in such quasi-two-dimensional systems. One regime, the fractional quantum Hall regime, is characterized by new quasiparticles, so-called composite fermions [3]. Manifestations of fundamentally new interaction effects have also been found in quasi-one-dimensional systems, both in charge density wave systems and in conducting polymers like polyacetylene. For polyacetylene, which is also a quasi-one-dimensional system as it is a long conjugated polymer, it was proposed some two decades ago that the electron-phonon interaction is essential for understanding many of its physical properties [4]. In this case, the lowest energy excitations are a combination of a localized lattice distortion and a localized electronic state — these so-called solitons are new topological excitations which can also be viewed as quasi-particles with nontrivial spin and charge quantum numbers.

These few examples serve to illustrate that fermionic correlation effects can manifest themselves in a variety of ways, and in a variety of systems. This is

reflected in this thesis, in which we consider two different, unrelated actually, examples of such fermionic correlations. The first one is a phenomenological approach that has been proposed to describe the normal state of high-T_c superconductors. This so-called Marginal Fermi Liquid approach [5] was introduced a number of years ago to capture a number of salient experimental features of the high-T_c materials in a few formulas. The second topic of this thesis will be the development of a simple extension of the Su-Schrieffer-Heeger model for polyacetylene to include the torsional and twist degrees of freedom. The aim of this study is to arrive at a model in the spirit of the Su-Schrieffer-Heeger model to describe the coherent conformational dynamics of (bio)molecules like retinal, the molecule that plays an important role in the first steps in vision. Below we motivate these two major themes of this thesis in more detail.

1.1 The Marginal Fermi Liquid phenomenology

The Marginal Fermi liquid approach was motivated by the observation that the anomalous normal-state properties of the high-temperature superconductors near optimal doping, like the linear-in-temperature resistivity over a large temperature range and the linear-in-frequency width of the quasiparticle peaks in photoemission experiments, could be modelled empirically by postulating that the imaginary part of the self-energy behaves as

$$\mathrm{Im}\Sigma(\omega, T) = (\lambda\pi/2)\max(\omega, T). \tag{1.1.1}$$

When starting from the marginal Fermi liquid Ansatz for the polarizability, as proposed by Varma *et al.* [5], one obtains $\lambda = g^2 N(0)^2$, g being a coupling constant and $N(0)$ the density of states at the Fermi energy. This relation between the polarizability and the self-energy is discussed further in the first appendix to chapter 2.

If still valid in the limit of zero temperature and frequency, a regime which actually is hidden due to the occurrence of superconductivity in the cuprates, this behavior would imply a just-breakdown of the quasi-particle concept. The name "marginal Fermi liquid" derives from this condition. If, on the other hand, a small energy scale exists in the system, for instance due to low-lying spin fluctuations, it might well be possible that the anomalous normal state properties are consistent with a Fermi liquid-like picture below this small energy scale. In this case, they would not really imply a breakdown of the quasi-particle concept in the cuprates [6].

In either case, however, strong inelastic scattering dominates the physics of the normal state. It has been pointed out that this inelastic scattering in the normal state largely affects the superconducting state: first of all the transition temperature is lowered substantially as a consequence of pairbreaking [7–10]. Secondly, the suppression of coherence peaks and a steep behavior of the gap,

with an enhanced value of $2\Delta(0)/k_BT_c$, might arise as consequences of a strong temperature dependence of the inelastic scattering rate below T_c [7-11].

It is aesthetically most attractive to assume that the physics underlying the anomalous normal state behavior of the cuprates is also the origin of the superconductivity [12], or is strongly competing with it. Kuroda and Varma [11] and Littlewood and Varma [13] have pursued the first possibility in an Eliashberg strong-coupling approach, in which the MFL-polarizability plays the role of the bosonic mode that is responsible for the superconductivity, i.e. where the MFL-polarizability replaces the usual electron-phonon coupling $\alpha^2F(\omega)$. They find s-wave superconductivity with an enhanced ratio $2\Delta(0)/k_BT_c$ and a sharply decreasing nuclear relaxation rate $1/T_1T$ below T_c rather than a coherence peak.

In chapter 2 we shall show, without referring to any specific theory about the origin of the superconductivity, that the superconducting state is very much affected by the normal state behavior described by the MFL Ansatz or the suppression thereof in the superconducting state. We demonstrate this by analyzing the effect of an additional attractive BCS-type potential on a system in which the *dominant* scattering causes the unusual normal state behavior. The transition temperature T_c for this case can be determined from the ladder instability of the normal state. Below T_c, when the gap opens up, the suppression of the (electronic) bosonic mode is modeled by a scattering rate that decreases with decreasing temperature. The gap at zero temperature, $\Delta(0)$, remains practically unaffected by the MFL behavior above T_c if the MFL scattering is sufficiently suppressed at $T = 0$. Consequently, the ratio $2\Delta(0)/k_BT_c$ is enhanced even for a weak-coupling superconductor, and the gap opens up rapidly; even a discontinuous first order transition at T_c is possible. Furthermore, we find that this behavior of the gap together with the smearing of the singularity in the BCS density of states due to the MFL scattering suppresses the coherence peaks.

Although the *dominant* scattering leads to anomalous normal state behavior modelled by the MFL Ansatz, a weaker interaction can be the origin of the superconductivity if retardation effects play a role, i.e. if different interactions involve different time scales. Within our description it is quite possible that the anomalous properties of the superconducting state of the cuprates are mainly due to the fact that the pairing occurs in a strongly correlated system (with MFL behavior), and that they are only weakly related to the origin of the pairing. Indeed, our results demonstrate a large degree of insensitivity of the unusual superconducting properties to the pairing mechanism. This becomes especially apparent by comparing our results to those of Littlewood and Varma [13], which are very similar, but obtained with the MFL-boson taken as the origin of the superconductivity.

Our investigation of the consequences of unusual normal state behavior modelled by the MFL Ansatz thus nicely illustrates two simple generic features of high-T_c materials: first of all, it shows that the rapid suppression of the quasiparticle scattering rate below T_c will automatically lead to a relatively high ratio

of $2\Delta/k_BT_c$. A large value of this ratio is normally associated with strong coupling effects, but our analysis illustrates that this conclusion can not be drawn automatically. Although this is implicit in other more sophisticated approaches, like the one taken by Kuroda and Varma [11], the simplicity of our analysis brings this point to the foreground. Secondly, our analysis of marginal Fermi liquid effects on the fluctuation contribution to the conductivity, which is the subject of chapter 3, shows that these fluctuations are suppressed. Hence, while in the superconducting phase fluctuation effects in these materials are strongly enhanced due to the combined effect of the short coherence length, the high transition temperature and the strong anisotropy — taken together, these changes are so important that a whole new field of vortex phase physics has emerged — the strong normal state scattering modelled by the MFL Ansatz has the opposite effect, namely a suppression of the fluctuation contribution to the conductivity.

When the work for this thesis was started, it appeared that the MFL approach could be a promising route towards a semi-quantitative understanding of a number of properties of the normal phase of the high-T_c materials, and that the Ansatz might help in pointing the road towards a more microscopic theory, by putting constraints on it. These original promises have not been fulfilled. As the Ansatz is a postulate on the outcome of a hypothetical intermediate step of a calculation, it is not really a self-consistent theory. Consequently, calculations involve (implicit) questionable assumptions and the form of the Ansatz tells little — if anything — about the microscopic origin of the anomalous normal state behavior. Moreover, within the Ansatz, the spin degrees of freedom play no role at all, while in recent years it has become undeniable that the physics of the high-T_c materials is associated with a strong interplay between charge and spin degrees of freedom — for example, there is now strong experimental evidence for the existence of striped phases, in which holes order in domain walls that separate spin ordered domains [14]. Furthermore, the fact that there is now strong evidence that the superconducting order parameter has d-wave symmetry also points at a strong interplay between spin and charge degrees of freedom. For these reasons, we decided not to continue the research on the marginal Fermi liquid approach which was the main research theme during the first phase of our work, and whose results are described in chapters 2 and 3.

1.2 The Su-Schrieffer-Heeger model for finite chains

As was already mentioned briefly before, the Su-Schrieffer-Heeger (SSH) Hamiltonian has proven to be a successful theoretical framework for understanding conjugated polymer chains [4,15,16]. In this tight-binding model one focusses on the coupling between the π-electrons that constitute the valence band, and the ionic motions along the one-dimensional polymeric chain. This model ex-

hibits a rich variety of nonlinear phenomena and topological excitations, which result from the existence of two possible and equivalent configurations of bond-length alternation in the Peierls distorted ground state.

The semi-classical dynamics following the excitation of a π-electron from the top of the valence band into the bottom of the conduction band in the dimerized ground state, has been the subject of a number of papers [17–20]. However, in these works kink-antikink generation and their dynamics was considered on chains of effectively infinite length only, using periodic boundary conditions; therefore, little is known about finite-size effects [21].

Our motivation for studying these kink–antikink excitations on chains of finite length comes from a somewhat unexpected corner, and was triggered by interactions and discussions with dr. H. J. M. de Groot from the chemistry department in Leiden. In biochemistry one encounters small light-harvesting molecules called "chromophores" that trigger a (not yet fully determined) sequence of steps after photo-excitation. A specific example of such a chromophore is the relatively small conjugated molecule 11-*cis*-retinal that has a carbon backbone of five ($C - C = C$)-units, and which is bound inside the protein opsin to form the light-sensitive rhodopsin. Rhodopsin is present in membranes of the rod cells of vertebrate retina, thereby enabling perhaps the most important sense: vision.

In recent years (bio)chemists have been slowly uncovering the secrets of vision and now some aspects of the first steps in vision seem well established. To be more specific, photo-excitation of this chromophore leads to an intermediate state (which is called bathorhodopsin) on an extremely short time scale, of the order of 200 femtoseconds [22]. On this time scale the chromophore undergoes a cis-to-trans isomerization; all other processes, which eventually lead to the triggering of a nerve signal, take place on much larger time-scales. To study this system theoretically, one has to come up with a definite model. Because of the fact that many details of the structure and function of rhodopsin are not yet known and that it is unclear precisely which details are relevant to the functioning of rhodopsin, a complete model obviously is a tall order. It does seem clear however, that an extension of the SSH model (taking into consideration torsional degrees-of-freedom) is well suited because of the fact that the chromophore itself is a small *conjugated* molecule. The SSH model is also a model of intrinsic simplicity and one in which kink–antikink excitations are consistent with both the short time scale and the high quantum yield. In fact there are experimental indications that the charge distributions in the neighbourhood of a charged nitrogen group on the retinal, are described quite well by the SSH Hamiltonian with Coulomb corrections. Moreover, ab initio calculations by Bifone *et al.* [23] in the group of de Groot, also give indications for solitonic type of excitations if retinal is artificially brought into a twisted state. In such type of calculations, however, excited states can not properly be studied; in addition, the temporal dynamics can not be studied within such an approach, whereas tight binding type models of the kind we will introduce in chapters 4 and 5 are ideally suited

to do so: simulations of our model for short to medium size chains can easily be run on a standard workstation.

Studying the effects of finite chain-lengths on the kink-antikink dynamics within the SSH model is a modest but logical first step towards the understanding of the first step in vision. So before we can turn our attention to the formulation of a tight-binding type model that allows us to study the dynamics of the untwisting of retinal in chapter 5, it is necessary to analyse more precisely how to study chains of finite length within the framework of an SSH-type model. It is this issue which is the subject of chapter 4. In order to study chains of finite length without periodic boundary conditions, the question arises as to which boundary condition to use, *e.g.* whether to leave the chain ends open, or to use a potential at the outer ends to regulate the chain length. Although this question has arisen before, it has, to our knowledge, not been addressed systematically. A study of these effects therefore turned out to be an essential ingredient for reaching our long term goal.

Our analysis in chapter 4 relies on a general expression that we derive for the energy-per-site $\varepsilon(u, \delta)$ of the SSH model, for uniform but arbitrary values of the dimerization amplitude u and bond stretching δ. We show that a careful but relatively straightforward evaluation of $\varepsilon(u, \delta)$ for a finite and open SSH chain allows one to determine the proper boundary conditions such that the bulk properties (ground state dimerization amplitude $\underline{u}$ and stretching $\underline{\delta}$) of long but open SSH chains are the same as those of periodic chains for the same parameter sets. This facilitates comparison of results for the two types of boundary conditions. Furthermore, the central rôle of the energy-per-site $\varepsilon(u, \delta)$ is made even more apparent when we consider the velocity of sound within the SSH model. In chapter 4 we will show how, both in a heuristic and in a more formal manner, a non-perturbative expression for the velocity of sound as a function of the electron-phonon coupling strength in the SSH model can be obtained.

In chapter 5, we briefly introduce our extension of the SSH model, which allows us to describe the dynamics of a molecule embedded in a three-dimensional space. To arrive at this extension, we have to account for the fact that the overlap of π-orbitals on adjacent sites — and hence the hopping rate of the electrons in the π-band — depends on the relative angle between these π-orbitals. Moreover, we have to allow for bond bending, the fact that the lobes of bonding σ-orbitals may point in directions that differ slightly from $2\pi/3$ radians. The new constants appearing in our extension, like the bond-bending elastic constant, can be determined relatively accurately by comparing the frequencies of the vibrational modes with typical values reported in the literature. For this reason, the normal mode analysis of our model, summarized in chapter 5, is an important ingredient for fixing these parameters.

Although a full study of our model has not been completed yet, our results so far indicate that it is a viable model for studying the coherent dynamics and conformational changes in small and medium sized linear conjugated molecules.

Once the parameters are fixed by comparing the results of our normal mode analysis to experimental vibration frequencies, our model yields explicit results, not only for the dynamics of molecules like the retinal in rhodopsin, but also for the energies of different (meta)stable states of molecules. Our preliminary investigations along these lines make us hopeful that our model does capture an important part of the physics involved: as we will discuss in chapter 5, the lowest vibrational period of a molecule with a size comparable to the size of retinal is of order 385 femtoseconds. Given the fact that our model does not take into account many features of the molecule and its surrounding protein cage that might have some influence, this compares favourably well with the 550 femtoseconds oscillations that have been seen in the absorption spectra after photoexcitation of the molecule. An immediate implication of this comparison is that this slow oscillation is primarily a *bending* mode, not a twist mode. As an example of the other way in which our model can be tested, we note that as yet unpublished results for cyclooctatetraene (COT) indicate that our model gives quite reasonable results for the energy difference between the "boat" and "chair" configuration of this molecule [24].

In the model we have developed so far, we have not included a Hubbard type of interaction term. For the soliton excitations that arise in the one-dimensional SSH model, it is known that these Hubbard type of interaction terms can be taken into account perturbatively (provided the Hubbard-U interaction is not too large, of course), and it does not change the qualitative physics. One may wonder whether this remains true when one analyses the strong twists that necessarily occur during conformational changes. This question is presently being investigated by Aalberts and coworkers. With a Hubbard interaction term, the model does become computationally more intensive, but with the recent advances in treating strongly correlated quasi-one-dimensional quantum systems using the Density Matrix Renormalization Group method, it appears that inclusion of such terms is within reach [25]. This opens up a whole new avenue for treating chainlike molecular systems and for which our model in chapter 5 provides a basis.

Bibliography

[1] N. W. Ashcroft and N. D. Mermin, *Solid State Physics*, Saunders College Publishing, 1988.

[2] P. Nozières and D. Pines, *The Theory of Quantum Liquids*, Addison-Wesley Publishing Co., Inc., 1989.

[3] R. E. Prange and S. M. Girvin eds., *The Quantum Hall Effect*, Springer-Verlag, 1987.

[4] A.J. Heeger, S. Kivelson, J.R. Schrieffer and W.P. Su, Rev. Mod. Phys. **60**, 781 (1988).

[5] C.M. Varma, P.B. Littlewood, S. Schmitt-Rink, E. Abrahams and A.E. Ruckenstein, Phys. Rev. Lett. 63, 1996 (1989).

[6] W.W. Warren,Jr., R.E. Walstedt, G.F. Brennert, G.P. Espinosa and J.P. Remeika, Phys. Rev. Lett. 59, 1860 (1987); P.C. Hammel, M. Takigawa, R.H. Heffner, Z. Fisk and K.C. Ott, Phys. Rev. Lett. 63, 1992 (1989).

[7] G. Grüner, in *Phenomenology and applications of high-temperature superconductors*, editors K.S. Bedell et al., Addison Wesley (1992)

[8] M. Nuss, P.M. Mankiewicz, M.L. O'Malley, E.H. Westerwick, and P.B. Littlewood, Phys. Rev. Lett 63, 3305 (1991); M.L. Horbach and W. van Saarloos, Phys. Rev. B46, 432 (1992).

[9] Z. Schlesinger, R.T. Collins, F. Holtzberg, C. Feild, G. Koren and A. Gupta, Phys. Rev. B41, 11237 (1990); M. Boekholt, M. Hoffmann and G. Güntherodt, Physica C175, 127 (1991); Yonghong Li, Jin Lin Huang and C.M. Lieber, Phys. Rev. Lett. 68, 3240 (1992).

[10] D.A. Bonn, P. Dosanjh, R. Liang and W.N. Hardy, Phys. Rev. Lett. 68, 2390 (1992).

[11] Y. Kuroda and C.M. Varma, Phys. Rev. B42, 8619 (1990).

[12] P.W. Anderson, in *Frontiers and Borderlines in Many-Particle Physics*, editors R.A. Broglia and J.R. Schrieffer, North-Holland (1988).

[13] P.B. Littlewood and C.M. Varma, Phys. Rev. B46, 405 (1992); P.B. Littlewood and C.M. Varma, J. Appl. Phys. 69, 4979 (1991).

[14] J. Zaanen, M. L. Horbach and W. van Saarloos, Phys. Rev. B53, 8671 (1996).

[15] Yu Lu, *Solitons & Polarons in Conducting Polymers* (World Scientific, Singapore 1988).

[16] D. Baeriswyl, in *Theoretical Aspects of Band Structures and Electronic Properties of Pseudo-One-Dimensional Solids*, ed. H. Kamimura, (Reidel 1985).

[17] W.P. Su and J.R. Schrieffer, Proc. Natl. Acad. Sci. USA **77**, 5626 (1980).

[18] E.J. Mele, Solid State Comm. **44** , 827 (1982).

[19] E.J. Mele, Phys. Rev. B **26**, 6901 (1982).

[20] F. Guinea, Phys. Rev. B **30**, 1884 (1984).

[21] One study of finite molecules is: J.L. Brédas and A.J. Heeger, Chem. Phys. Lett. **154**, 56 (1989). For short molecules in the first electronically excited state, they study the size-dependence of relaxed solitonic steady-states. [See also J.L. Brédas, J.M. Toussaint, and A.J. Heeger, Mol. Cryst. Liq. Cryst. **189**, 81 (1990).]

[22] R.W. Schoenlein, L.A. Peteanu, R.A. Mathies and C.V. Shank, Science **254**, 412 (1991).

[23] A. Bifone, H. J. M. de Groot and F. Buda, Pure & Appl. Chem., 69, 2105 (1997), and references therein.

[24] D.P. Aalberts, F.L.J. Vos and W. van Saarloos, *in preparation.*

[25] C. Zhang, E. Jechelmann and S.R. White, cond-mat/9709187 (1997).

2 Phenomenology of the Superconducting State of a Marginal Fermi Liquid with BCS Model-Interaction

2.1 Introduction

Since the discovery of high-temperature superconductors a decade ago, much theoretical effort has been made to understand the peculiar properties that these materials display. The superconducting state of the high-temperature superconductors shows a number of unusual features in comparison with weak-coupling BCS superconductors. Most prominent in the early days were the absence of coherence peaks in the nuclear spin relaxation rate $1/T_1T$ [1] and also in the conductivity $\sigma_1(\omega)$ [2] (though in the latter quantity peaks arising from lifetime effects or thermal fluctuations can appear [3]), and an unusually large ratio $2\Delta(0)/k_BT_c$, for which values up to 10 have been reported [4]. In recent years it has, in addition, become clear that these high-T_c materials are d-wave superconductors and not s-wave superconductors like the classical materials.

Furthermore, the normal-state properties of the high-temperature superconductors near optimal doping, like the linear-in-temperature resistivity over a large temperature range and the linear-in-frequency width of the quasiparticle peaks in photoemission experiments, are anomalous with respect to normal metals.

Although there is no agreement yet on the microscopic description of these materials, it is believed by almost all workers in the field that the origin of the superconductivity and the anomalous normal-state properties are intimately linked. In an attempt to give a unified perspective on the experimental facts, a phenomenological approach was taken by Varma *et al.* [5]. They showed, that the unconventional normal-state behavior was well described by the marginal Fermi liquid (MFL) hypothesis. Most of the anomalous normal-state properties can, according to this hypothesis, be understood from a single assumption about the polarizability of the (strongly interacting) system, namely

$$\mathrm{Im}P(\vec{q},\omega) \propto \tanh(\omega/T)\,. \tag{2.1.1}$$

It leads for instance to an electronic scattering rate $1/\tau = (\lambda\pi/2)\max(T,|\omega|)$, where $\lambda = g^2N(0)^2$, with g being the coupling of the electrons with the unidentified excitations that lead to the unusual polarizability and $N(0)$ the density of states at the Fermi energy.

The assumption that the dominant scattering occurs by exchange of the excitations that give rise to the unusual polarizability immediately leads to the

observation that below T_c, as the gap opens up, this scattering proces will be suppressed considerably (most dramatically if the coupling of the electrons to the polarizability is such that it leads to type I coherence factors). As a consequence the quasi-particle lifetime will rapidly increase as the temperature is lowered. Measurements of the surface resistance of YBCO [6] do indeed appear to give evidence for a suppression of the quasiparticle scattering rate, and hence support the assumption about the dominant role of an electronic scattering process involving a nontrivial renormalization of the polarizability.

As we mentioned in the introductory chapter, it is aesthetically most attractive to assume that the (yet unknown) physics underlying the MFL hypothesis is also the origin of the superconductivity [7]. Kuroda and Varma [8] and Littlewood and Varma [9] have pursued this idea in an Eliashberg strong-coupling approach, in which the MFL-polarizability plays the role of the bosonic mode that is responsible for the superconductivity, i.e. where the MFL-polarizability replaces the usual electron-phonon coupling $\alpha^2 F(\omega)$. They find s-wave superconductivity with an enhanced ratio $2\Delta(0)/k_B T_c$ and a sharply decreasing $1/T_1 T$ below T_c rather than a coherence peak.

However, in this chapter we shall show, without referring to any specific theory about the origin of the superconductivity, that the superconducting state is very much affected by the normal state MFL-behavior. We demonstrate this by analyzing the effect of an additional attractive BCS-type potential on a system in which the *dominant* scattering causes MFL behavior. The transition temperature T_c for this case can be determined from the ladder instability of the normal state. Below T_c, when the gap opens up, the suppression of the (electronic) bosonic mode is modeled by a scattering rate that decreases with decreasing temperature. The gap at zero temperature, $\Delta(0)$, remains practically unaffected by the MFL behavior above T_c if the MFL scattering is sufficiently suppressed at $T = 0$. Consequently, the ratio $2\Delta(0)/k_B T_c$ is enhanced even for a weak-coupling superconductor, and the gap opens up rapidly; even a discontinuous first order transition at T_c is possible. Furthermore, we will find that this behavior of the gap together with the smearing of the singularity in the BCS density of states due to the MFL scattering suppresses the coherence peaks.

Although the *dominant* scattering leads to MFL behavior a weaker interaction can be the origin of the superconductivity if retardation effects play a role, i.e. if different interactions involve different time scales. It is therefore quite possible that the anomalous properties of the superconducting state of the cuprates are mainly due to the fact that the pairing occurs in a strongly correlated system (with MFL behavior), and that they are only weakly related to the origin of the pairing. Indeed, our results demonstrate a large degree of insensitivity of the unusual superconducting properties to the pairing mechanism. This becomes especially apparent by comparing our results to those of Littlewood and Varma [9], which are very similar, but obtained with the MFL-boson taken as the origin of the superconductivity.

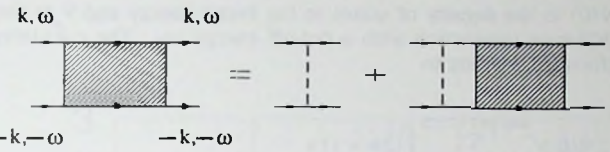

Figure 2-1. The particle-particle ladder. The dashed lines denote simple BCS -interactions, the propagators have a marginal Fermi liquid self-energy.

2.2 $2\Delta(0)/k_BT_c$ and suppression of T_c

With the simple model form for the attractive BCS interaction (up to an energy ω_0) T_c can be determined from the ladder instability of the normal-state. Here we neglect differences between the pair-formation temperature and the actual transition temperature. We take the normal-state propagators with the MFL self-energy. The form of this self-energy can be derived from the Ansatz for the polarizability (Eq. 2.1.1). The derivation is given in appendix A, with the result:

$$\Sigma(\vec{k},\omega) = \lambda[\omega \ln(x/\omega_c) - i(\pi x/2)]\,. \tag{2.2.1}$$

Here $x = \max(|\omega|, T)$ and ω_c is a large cut-off scale, which is estimated to be of the order of 0.5 eV from Raman scattering [1]; also the infrared measurements of Rotter *et al.* [10], which show a quasiparticle scattering rate which is linear in ω up to frequencies of 3000 cm^{-1} (0.37 eV) indicate a cut-off of this order. The value of λ can be determined from resistivity measurements. Taking from ref. [11] the result of resistivity measurements up to 600K on $Bi_2Sr_{2.2}Ca_{0.8}Cu_2O_8$ that $d\rho(T)/dT = 0.46\mu\Omega$cm/K , we find $\lambda = 0.23$, assuming a plasma frequency of 1 eV. Though the value of λ is certainly not the same for all high-T_c materials, it is of this order of magnitude.

The temperature Green function in the normal state then is

$$G(\vec{k}, i\omega_n) = [i\omega_n - \epsilon(\vec{k}) - \Sigma(i\omega_n)]^{-1}, \tag{2.2.2}$$

where from analytic continuation of the marginal Fermi liquid $\Sigma(\vec{k},\omega)$ it follows that (see appendix B)

$$\Sigma(i\omega_n) = -i\lambda T \arctan\left(\frac{T}{\omega_n}\right) - \frac{1}{2}i\lambda\omega_n \log\left(\frac{\omega_n^2+\omega_c^2}{\omega_n^2+T^2}\right). \tag{2.2.3}$$

The pairing-instability occurs at the temperature where the particle-particle scattering amplitude $\Gamma(\vec{k},\omega,\vec{k},\omega;-\vec{k},-\omega,-\vec{k},-\omega)$ diverges (Fig. 2-1) [12],

$$1 = N(0)VT \sum_{|\omega_n|<\omega_0} \int d\epsilon(\vec{k}) G(-\vec{k}, -i\omega_n) G(\vec{k}, i\omega_n)\,, \tag{2.2.4}$$

where $N(0)$ is the density of states at the Fermi energy and V is the strength of the BCS-type interaction with a cut-off energy ω_0. The $\epsilon(\vec{k})$-integration is straightforward, leading to

$$1 = 2N(0)V \sum_{n=0}^{\omega_0/2\pi T-(1/2)} \Bigg[(2n+1)\times \tag{2.2.5}$$

$$\times\left(1+\frac{\lambda}{2}\log\left(\frac{(2n+1)^2\pi^2T^2+\omega_c^2}{(2n+1)^2\pi^2T^2+T^2}\right)+\frac{\lambda}{(2n+1)\pi}\arctan\left(\frac{1}{(2n+1)\pi}\right)\right)\Bigg]^{-1}.$$

The remaining sum over the Matsubara frequencies can, under the condition that $\omega_0 < \omega_c$ or that λ is sufficiently small, be approximated by

$$2N(0)V \sum_{n=0}^{\omega_0/2\pi T-(1/2)} \frac{1}{(2n+1)\,[1-\lambda\log((2n+1)\pi T/\omega_c)]}$$

$$\approx 2N(0)V \sum_{n=0}^{\omega_0/2\pi T-(1/2)} \frac{1}{(2n+1)\,[1+\lambda\log(\omega_c/\pi T)]}\left[1+\frac{\lambda\log(2n+1)}{1+\lambda\log(\omega_c/\pi T)}\right]. \tag{2.2.6}$$

Performing the sum in the first contribution from the term between square brackets and writing the second sum as an integral gives the instability condition, which can be written as a quadratic equation for $\log(\omega_0/\pi T_c) \equiv X$, $AX^2 + BX + C = 0$, with the coefficients

$$A \equiv \frac{5\lambda}{4} - \frac{\lambda^2}{N(0)V}$$

$$B \equiv -\frac{2\lambda}{N(0)V}(1-\lambda\log\alpha) - \lambda\left(\log 2+\psi\left(\frac{1}{2}\right)\right)+(1-\lambda\log\alpha),$$

$$C \equiv -\frac{1}{N(0)V}(1-\lambda\log\alpha)^2 - \left(\log 2+\psi\left(\frac{1}{2}\right)\right)(1-\lambda\log\alpha)). \tag{2.2.7}$$

Here $\psi(x)$ is the Digamma function and $\alpha \equiv \omega_0/\omega_c < 1$. The critical temperature then is found to be

$$T_c(\lambda) = \frac{\omega_0}{\pi}\exp\left[\frac{B-\sqrt{B^2-4AC}}{2A}\right]. \tag{2.2.8}$$

Taking for instance $\lambda = 0.23$, ω_0=0.2 eV, ω_c=0.5 eV and $N(0)V$=0.5 yields T_c=91 K. In the limit $\lambda \to 0$ one recovers the BCS critical temperature, $T_c^{BCS} = 1.13\omega_0\exp[-1/N(0)V]$, which is higher than $T_c(\lambda > 0)$. In figure 2-2 we have plotted $T_c(\lambda = 0)/T_c(\lambda_{ns})$ as a function λ_{ns} for different values of $N(0)V$ and with $\alpha = 0.4$. One sees that the stronger the BCS-coupling is, the smaller the relative suppression of T_c due to the MFL-scattering. Thus the critical temperature is suppressed as compared to the BCS-value by the MFL-behavior of the normal

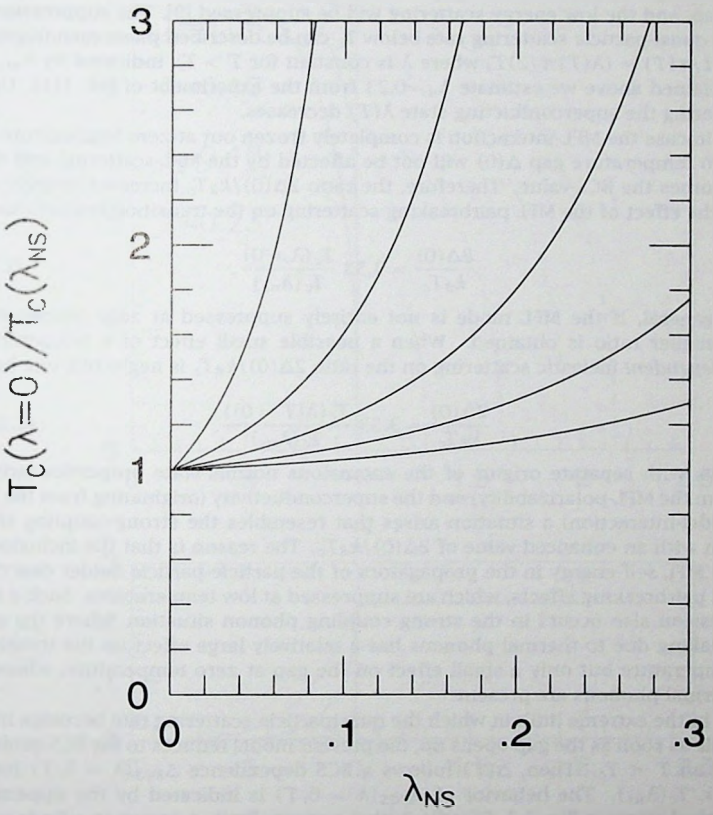

Figure 2-2. $T_c(\lambda = 0)/T_c(\lambda_{ns})$ versus $T_c(\lambda_{ns})$. The different curves correspond, from top to bottom, with values of $N(0)V$=0.3, 0.45, 0.6, 0.75 and 0.9.

state. This is a natural consequence of the pairbreaking caused by the inelastic MFL-scattering.

An immediate consequence of the electronic origin of the MFL-mode is that at low temperatures where the gap develops, the MFL-mode itself will also develop a gap, and the low energy scattering will be suppressed [9]. The suppression of the quasi-particle scattering rate below T_c can be described phenomenologically by $1/\tau(T) = (\lambda(T)\pi/2)T$, where λ is constant for $T > T_c$, indicated by λ_{ns}. As explained above we estimate λ_{ns}=0.23 from the experiment of ref. [11]. Upon entering the superconducting state $\lambda(T)$ decreases.

In case the MFL-interaction is completely frozen out at zero temperature the zero temperature gap $\Delta(0)$ will not be affected by the MFL-scattering and thus assumes the BCS-value. Therefore, the ratio $2\Delta(0)/k_BT_c$ increases entirely due to the effect of the MFL pairbreaking scattering on the transition temperature,

$$\frac{2\Delta(0)}{k_BT_c} = 3.53\,\frac{T_c(\lambda = 0)}{T_c(\lambda_{ns})}. \tag{2.2.9}$$

In general, if the MFL mode is not entirely suppressed at zero temperature, a smaller ratio is obtained. When a possible small effect of a temperature-*independent* inelastic scattering on the ratio $2\Delta(0)/k_BT_c$ is neglected, one has

$$\frac{2\Delta(0)}{k_BT_c} = 3.53\,\frac{T_c(\lambda(T = 0))}{T_c(\lambda_{ns})}. \tag{2.2.10}$$

Thus with separate origins of the anomalous normal-state properties (arising from the MFL-polarizability) and the superconductivity (originating from the BCS model-interaction) a situation arises that resembles the strong-coupling situation with an enhanced value of $2\Delta(0)/k_BT_c$. The reason is that the inclusion of the MFL self-energy in the propagators of the particle-particle ladder describes the pairbreaking effects, which are suppressed at low temperatures. Such a suppression also occurs in the strong coupling phonon situation, where the pairbreaking due to thermal phonons has a relatively large effect on the transition temperature but only a small effect on the gap at zero temperature, where no thermal phonons are present.

In the extreme limit in which the quasiparticle scattering rate becomes negligible as soon as the gap opens up, the present model reduces to the BCS-problem for all $T < T_c$. Then, $\Delta(T)$ follows a BCS dependence $\Delta_{BCS}(\lambda = 0, T)$ for all $T < T_c(\lambda_{ns})$. The behavior of $\Delta_{BCS}(\lambda = 0, T)$ is indicated by the uppermost dashed curve in Fig. 2-3. Clearly, in this extreme limit, Δ jumps to a finite value at $T_c(\lambda_{ns})$. In the general case in which the quasiparticle scattering rate remains nonvanishing below T_c, the opening up of the gap is less drastic, but still more rapid than in the BCS case: the quicker $\lambda(T)$ decreases below T_c, the quicker the gap opens up, and vice versa. Although in principle the full complex gap equations have to be solved below T_c to study this behavior, the general trend can be understood as follows. Consider a temperature-independent λ; for a given

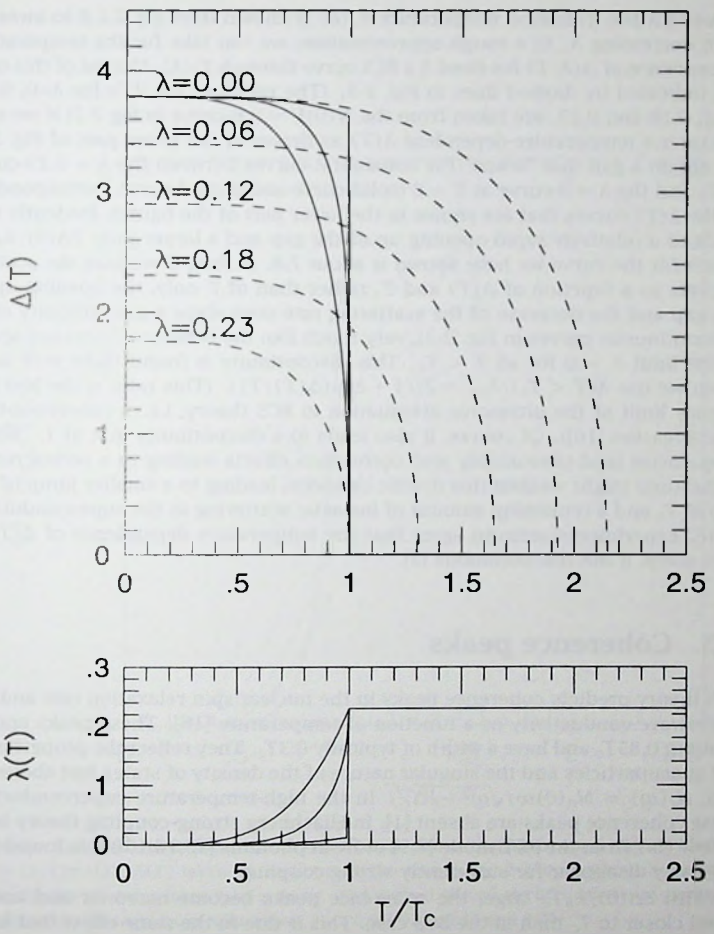

Figure 2-3. The gap as a function of temperature (upper figure) with a temperature-dependent λ (lower figure) with $2\Delta(0)/k_BT_c \approx 7.8$. The curves in the lower figure correspond to curves in the upper figure: the lower the $\lambda(T)$ curve, the higher the $\Delta(T)$ curve. The dashed lines are BCS curves (thus with $2\Delta(0)/k_BT_c = 3.53$) through $T_c(\lambda)$, with the values of λ given in the figure. We used $N(0)V$=0.6, ω_c = 0.5 eV and ω_0 = 0.2 eV.

value of λ the transition temperature $T_c(\lambda)$ is known from Eq. 2.2.8 to increase with decreasing λ. In a rough approximation, we can take for the temperature dependence of $\Delta(\lambda, T)$ for fixed λ a BCS curve through $T_c(\lambda)$. Curves of this type are indicated by dashed lines in Fig. 2-3. (The ratios of the T_c's for λ=0, 0.06, 0.12, 0.18 and 0.23. are taken from the $N(0)V$ = 0.6-curve in Fig 2-2) If we now consider a temperature-dependent $\lambda(T)$ as drawn in the lower part of Fig. 2-3, we obtain a gap that "scans" the constant-λ-curves between the λ = 0.23-curve at T_c and the λ = 0-curve at T = 0 (solid curve and dotted curve, corresponding to the $\lambda(T)$ curves that are shown in the lower part of the figure). Evidently this leads to a relatively rapid opening up of the gap and a larger ratio $2\Delta(0)/k_BT_c$, which for the curve we have shown is about 7.8. In fact, if we take the scattering rate as a function of $\Delta(T)$ and T, rather than of T only, the opening up of the gap and the decrease of the scattering rate even show a discontinuity at T_c (discontinuous curves in Fig. 2-3), very much like the behavior discussed above in the limit $\lambda \to 0$ for all $T < T_c$. This discontinuity is found to be very large when we use $\lambda(T < T_c)/\lambda_{ns} = 2/(1 + \exp(\Delta(T)/T))$. (This ratio is the low frequency limit of the ultrasonic attenuation in BCS theory, i.e. a coherence-type I suppression [16]). Of course, it also leads to a discontinuity in λ at T_c. Finite frequencies (and presumably also correlation effects leading to a vertex renormalisation) might weaken this drastic behavior, leading to a smaller jump of the gap at T_c and a remaining amount of inelastic scattering in the superconductive state. Experiments seem to agree that the temperature dependence of $\Delta(T)$ is very steep, if not discontinuous [3].

2.3 Coherence peaks

BCS theory predicts coherence peaks in the nuclear spin relaxation rate and the microwave conductivity as a function of temperature [16]. These peaks appear at about $0.85T_c$ and have a width of typically $0.3T_c$. They reflect the properties of the quasi-particles and the singular nature of the density of states just above the gap, $N_s(\omega) = N_n(0)\omega/\sqrt{\omega^2 - |\Delta|^2}$. In the high-temperature superconductors these coherence peaks are absent [1]. In Eliashberg strong-coupling theory (with an $\alpha^2F(\omega)$ from the MFL mode [8,9] or from phonons [13,14,15]) it is found that they may disappear for sufficiently strong coupling.

With $2\Delta(0)/k_BT_c$ large, the coherence peaks become narrower and are located closer to T_c than in the BCS case. This is due to the same effect that leads to the steep behavior of the gap: As the parameter λ changes upon entering the superconductive state a scan of the BCS curves between the λ=0.23-curve at T_c and the λ=0-curve at T=0 (as described above for the gap) is made, as shown in Fig. 2-4. This yields a narrow coherence peak. By using directly the steep gap, one also finds this narrow coherence peak. With λ being a function of $\Delta(T)$, as was considered above, the coherence peak disappears completely when the

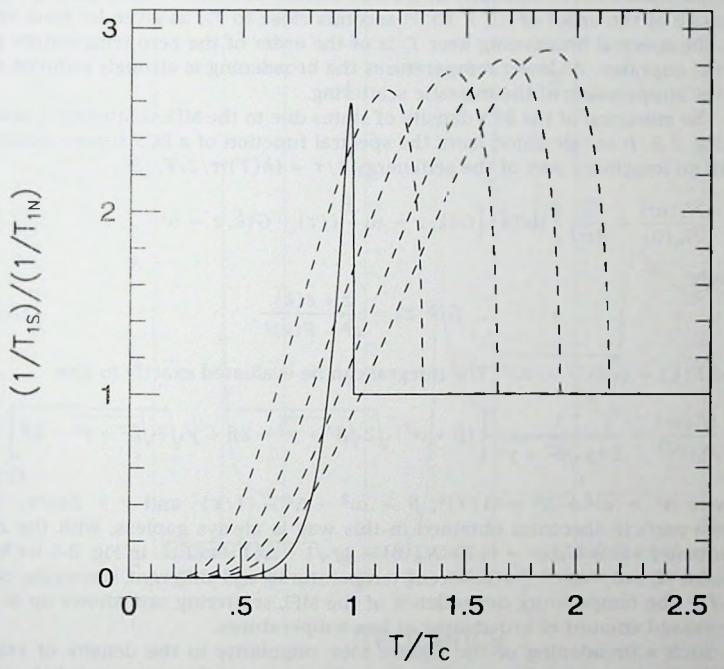

Figure 2-4. Coherence peak (solid curve) with a temperature dependent quasi-particle lifetime $1/\tau = (\lambda(T)\pi/2)T$, $\lambda(T)$ taken as the upper $\lambda(T)$-curve in Fig. 2-3, but without broadening of the density of states taken into account. The dashed curves are BCS coherence peaks, T_c determined by (8) with, from right to left, λ=0, 0.06, 0.12, 0.18 and 0.23.

discontinuity of the gap, and thus of λ at T_c is sufficiently large. If λ changes continuously at T_c, always a narrow peak remains. The same mechanism leads to a more rapid suppression of the ultrasonic attenuation rate below T_c.

Close to T_c, in the region of the narrow peak, the inelastic scattering is still active. This scattering, in addition to the BCS-interaction, has the effect of smearing the square root singularity in the BCS density of states. With a quasi-particle lifetime of the order of 0.2×10^{-13} seconds close to T_c, as given by Bonn et al. [6], the spectral broadening near T_c is of the order of the zero temperature gap in the cuprates. At lower temperatures the broadening is strongly reduced due to the suppression of the inelastic scattering.

The smearing of the BCS density of states due to the MFL scattering is shown in Fig. 2-5. It is calculated from the spectral function of a BCS superconductor, with an imaginary part of the selfenergy $1/\tau = (\lambda(T)\pi/2)T$, i.e.

$$\frac{N_s(\omega)}{N_n(0)} = \frac{1}{2\pi i}\int d\epsilon(\vec{k})\left[G(\vec{k}, z \to \omega - i/\tau) - G(\vec{k}, z \to \omega + i/\tau)\right], \qquad (2.3.1)$$

where

$$G(\vec{k}, z) = \frac{z + \epsilon(\vec{k})}{z^2 - E(\vec{k})^2}, \qquad (2.3.2)$$

and $E(\vec{k}) = \sqrt{\epsilon(\vec{k})^2 + |\Delta|^2}$. The integral can be evaluated exactly to give

$$\frac{N_s(\omega)}{N_n(0)} = \frac{1}{2\tau\gamma\sqrt{\beta^2+\gamma^2}}\left[(\beta+\alpha^2)\sqrt{2\sqrt{\beta^2+\gamma^2}+2\beta} + \gamma\sqrt{2\sqrt{\beta^2+\gamma^2}-2\beta}\right], \qquad (2.3.3)$$

where $\alpha^2 = \omega^2 + \Delta^2 + (1/\tau)^2$, $\beta = \omega^2 - \Delta^2 - (1/\tau)^2$ and $\gamma = 2\omega/\tau$. The quasi-particle spectrum obtained in this way is always gapless, with the zero frequency value $N_s(\omega - 0, T)/N_n(0) = 1/\sqrt{1 + \Delta(T)^2\tau(T)^2}$. In Fig. 2-5 we have shown $N_s(\omega)/N_n(0)$ for different temperatures and different scattering rates at T_c. The temperature dependence of the MFL scattering rate shows up in the decreased amount of broadening at low temperatures.

Such a broadening of the square root singularity in the density of states, which occurs especially near T_c, where the narrow coherence peak is located, suppresses the peak largely or totally, as is shown in Fig. 2-6. This suppression even occurs for scattering rates that are smaller by a factor of two than quoted above.

2.4 Conclusions

In this chapter, we have considered a system of electrons with an (unidentified) dominant scattering mechanism that leads to marginal Fermi liquid behavior and a BCS model-interaction, that causes superconductivity. In absence of the

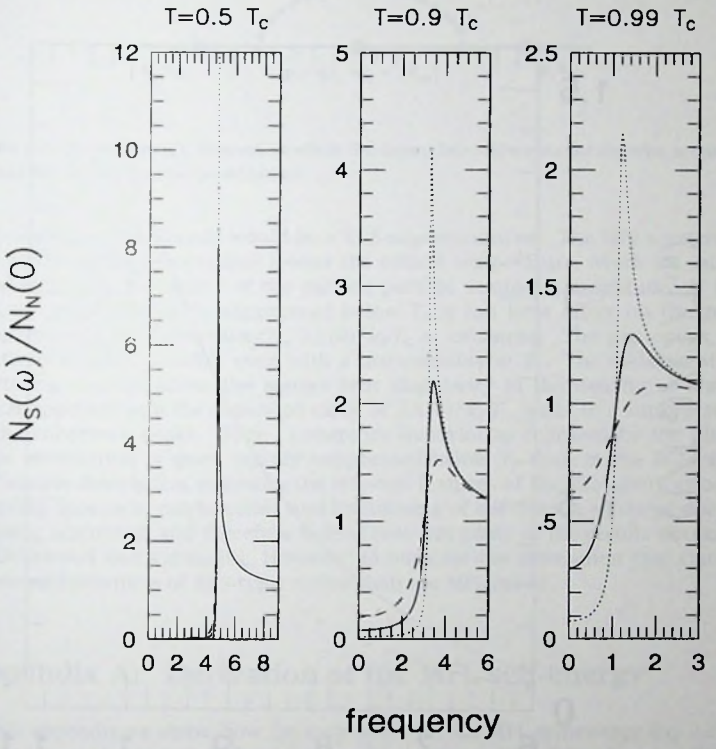

Figure 2-5. The density of states in the superconducting state with the MFL-interaction at different temperatures. At low temperatures the MFL-interaction is suppressed and the BCS square root singularity is recovered. At higher temperatures the MFL interaction is stronger, and the smearing of the singularity stronger.The dotted curve is obtained with a scattering rate of $0.02\times\Delta(0)$ at T_c, the solid line with a scattering rate of $0.05\times\Delta(0)$ at T_c and the dashed line with a scattering rate of $0.4\times\Delta(0)$ at T_c. We used a decrease of the scattering rate as indicated by the solid curve in Fig. 2-3, i.e. $\lambda(T) = (T/T_c)^4\lambda_{ns}$ below T_c. Even our largest scattering rate is modest compared to the one given by Bonn et al. [6].

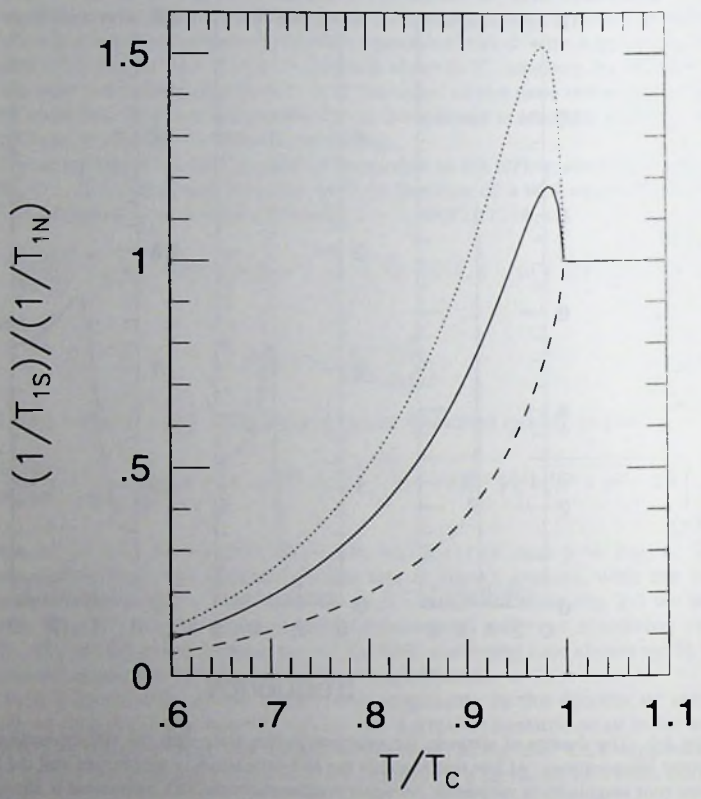

Figure 2-6. The nuclear spin relaxation rate $1/T_1$ normalized to the normal state value with broadening of the density of states taken into account. The scattering rates are the same as in figure refmfldos.

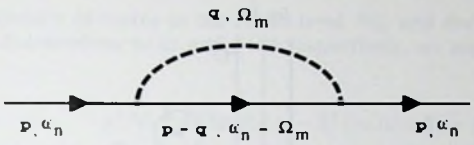

Figure 2-7. The self-energy diagram, in which the drawn line represents the electron propagator and the dashed line the polarization.

MFL-scattering the system would be a BCS-superconductor. The MFL-scattering is a pairbreaking process that lowers the critical temperature, which we calculated from the divergence of the particle-particle scattering amplitude. If the MFL mode is sufficiently suppressed below T_c it has little effect on the zero temperature gap. Consequently, $2\Delta(0)/k_BT_c$ is enhanced. The gap opens up relatively rapidly, possibly even with a discontinuity at T_c. The inelastic MFL-scattering also broadens the square root singularity in the density of states which, together with the enhanced value of $2\Delta(0)/k_BT_c$, leads to a suppression of the coherence peaks. Type I coherence behavior as followed by the ultrasonic attenuation is more rapidly suppressed below T_c than in the BCS-case. Our simple description embodies the relevant features of the Eliashberg strong-coupling approach: pairbreaking and broadening of the density of states due to inelastic scattering, and therefore indeed recovers many of the results obtained by Littlewood and Varma [9]. However, in our case the interaction that causes superconductivity is of BCS-type, rather than the MFL-mode.

Appendix A: Derivation of the MFL self-energy

In this appendix we show, how the expression for the MFL self-energy (Eq. 2.2.1) follows from the Ansatz in Eq. 2.1.1 for the polarizability of the system. Using the diagram shown in Fig. 2-7, we may write the expression for the self-energy as:

$$\Sigma(\mathbf{p}, i\omega_n) = g^2 \int \frac{d\mathbf{q}}{(2\pi)^3} T \sum_{i\Omega_m} \frac{P(\mathbf{q}, i\Omega_m)}{i\omega_n - i\Omega_m - \xi_{\mathbf{p}-\mathbf{q}}}. \tag{A.1}$$

The sum can be evaluated in the usual way, by representing the sum as an integral along the contour C shown in Fig. 2-8:

$$\Sigma(\mathbf{p}, i\omega_n) = \frac{g^2}{2\pi i} \int \frac{d\mathbf{q}}{(2\pi)^3} \oint_C d\omega' \frac{P(\mathbf{q}, \omega')}{i\omega_n - \omega' - \xi_{\mathbf{p}-\mathbf{q}}} \frac{1}{e^{\beta\omega'} - 1}. \tag{A.2}$$

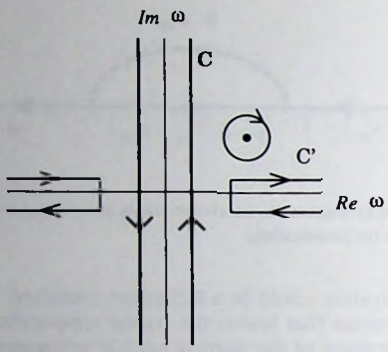

Figure 2-8. The contours used in Eqs. A.2 and A.3. The heavy lines denote the contour C, while the thin lines denote the contour C' into which C will be deformed.

As a second step, we deform the contour C into the contour C'. In doing so we obtain, in a shorthand notation:

$$\oint_C d\omega' = \oint_{C'} d\omega' = \mathcal{P}\int_{-\infty+i\delta}^{\infty+i\delta} d\omega' - \mathcal{P}\int_{-\infty-i\delta}^{\infty-i\delta} d\omega' - 2\pi i \,\mathrm{res}_{\omega'=i\omega_n-\xi}\,. \tag{A.3}$$

Abbreviating $\xi_{\mathbf{p}-\mathbf{q}}$ by ξ, and anticipating that the the polarizability in an MFL does not explicitely depend on momentum, the expression for the self-energy is thus given by:

$$\begin{aligned}\Sigma(i\omega_n) &= \frac{g^2}{2\pi i}\int \frac{d\mathbf{q}}{(2\pi)^3}\left[\mathcal{P}\int_{-\infty}^{\infty} d\omega' \frac{1}{e^{\beta\omega'}-1}\cdot\frac{P(\omega'+i\delta)-P(\omega'-i\delta)}{i\omega_n-\omega'-\xi}\right.\\ &\qquad\left. -2\pi i\frac{P(i\omega_n-\xi)}{e^{\beta i\omega_n-\beta\xi}+1}\right]\\ &= \frac{g^2}{\pi}\int \frac{d\mathbf{q}}{(2\pi)^3}\left[\mathcal{P}\int_{-\infty}^{\infty} d\omega' \frac{1}{e^{\beta\omega'}-1}\,\frac{\mathrm{Im}\,P_R(\omega')}{i\omega_n-\omega'-\xi} - \right.\\ &\qquad\left. \pi\frac{P(i\omega_n-\xi)}{e^{\beta i\omega_n-\beta\xi}+1}\right].\end{aligned} \tag{A.4}$$

Continuation to real frequency ($i\omega_n \to \omega + i\delta$) gives

$$\Sigma_R(\omega) = \frac{g^2}{\pi}\int \frac{d\mathbf{q}}{(2\pi)^3}\left[\int_{-\infty}^{\infty} d\omega' \frac{1}{e^{\beta\omega'}-1}\,\frac{\mathrm{Im}\,P_R(\omega')}{\omega-\omega'-\xi+i\delta} - \pi\frac{P_R(\omega-\xi)}{e^{\beta\omega-\beta\xi}+1}\right], \tag{A.5}$$

from which the imaginary part can be obtained as

$$\mathrm{Im}\,\Sigma_R(\omega) = -g^2\int \frac{d\mathbf{q}}{(2\pi)^3}\left[\frac{\mathrm{Im}\,P_R(\omega-\xi,\mathbf{q})}{e^{\beta(\omega-\xi)}-1} + \frac{\mathrm{Im}\,P_R(\omega-\xi,\mathbf{q})}{e^{-\beta\xi}+1}\right]. \tag{A.6}$$

Introducing the density of states at the Fermi level $\mathcal{N}_0$, and the Bose-Einstein and Fermi-Dirac distributions $n(x)$ and $f(x)$ respectively, we may rewrite this as

$$\begin{aligned} \mathrm{Im}\,\Sigma_R(\omega) &= -g^2\mathcal{N}_0 \int d\xi\, \mathrm{Im}\, P_R(\omega-\xi)\,[n(\omega-\xi)+f(-\xi)] \\ &\overset{\xi\to\omega-\xi}{=} -g^2\mathcal{N}_0 \int d\xi\, \mathrm{Im}\, P_R(\xi)\,[n(\xi)+f(\xi-\omega)]\,. \end{aligned} \tag{A.7}$$

Substituting for $\mathrm{Im}\, P_R$ the MFL form

$$\mathrm{Im}\, P_R(\xi) = -\mathcal{N}_0 \frac{\tanh(\xi/T)}{1+\xi^2/\omega_c^2}\,, \tag{A.8}$$

then finally leaves us with

$$\mathrm{Im}\,\Sigma_R(\omega) = \lambda \int d\xi\, \frac{\tanh(\xi/T)}{1+\xi^2/\omega_c^2}\,[n(\xi)+f(\xi-\omega)]\,, \tag{A.9}$$

where $\lambda = g^2\mathcal{N}_0^2$.

Although this integral cannot be evaluated analytically, it is easy to deduce its following properties:

- for $\omega << T << \omega_c$, the product containing the Fermi-Dirac distribution f will not contribute much, and the remaining part with the product containing the Bose-Einstein factor n will result in a contribution that grows linearly with T.
- for $T << \omega << \omega_c$, only the Fermi-Dirac term will contribute significantly with a result that grows linearly in ω.

This behavior leads to the analytic form for the MFL self-energy as given by Eq. 2.2.1, since the real part may be obtained simply from the Kramers-Kronig relation between the real and imaginairy parts of an analytic function.

Appendix B: Analytic continuation of the MFL self-energy

In this appendix we will fill in the steps that lead from the MFL selfenergy for real frequencies to the expression for this self-energy for imaginairy frequencies, Eq. 2.2.3.

The selfenergy at imaginairy frequencies, $\Sigma(i\omega_n)$, can be obtained from the imaginairy part of the (retarded) self-energy at real frequencies, $\Sigma_R''(\omega)$, through

$$\begin{aligned}\Sigma(i\omega_n) &= \frac{1}{\pi}\int_{-\infty}^{\infty} d\omega \frac{\Sigma_R''(\omega)}{\omega - i\omega_n} \\ &= \frac{1}{\pi}\int_{-\infty}^{0} d\omega \frac{\Sigma_R''(\omega)}{\omega - i\omega_n} + \frac{1}{\pi}\int_{0}^{\infty} d\omega \frac{\Sigma_R''(\omega)}{\omega - i\omega_n} \\ &= \frac{2i\omega_n}{\pi}\int_{0}^{\infty} d\omega \frac{\Sigma_R''(\omega)}{\omega^2 + i\omega_n^2},\end{aligned} \tag{B.1}$$

where, in the last step, use has been made of the fact that $\Sigma_R''(\omega)$ is an even function of ω.

Substitution of the MFL form

$$\Sigma_R''(\omega) = \frac{-\lambda\pi}{2}\left[T\theta(T - |\omega|) + \omega\theta(|\omega| - T)\right], \tag{B.2}$$

results in

$$\begin{aligned}\Sigma(i\omega_n) &= -i\lambda\omega_n\left\{\int_0^T d\omega \frac{T}{\omega^2 + i\omega_n^2} + \int_T^{\omega_c} d\omega \frac{\omega}{\omega^2 + i\omega_n^2}\right\} \\ &= -i\lambda T \arctan(\frac{T}{\omega_n}) - \frac{1}{2}i\lambda\omega_n \log\left(\frac{\omega_n^2 + \omega_c^2}{\omega_n^2 + T^2}\right),\end{aligned} \tag{B.3}$$

which is Eq. 2.2.3.

It is easily verified that this expression correctly returns the self-energy expression for real frequencies. Indeed, analytic continuation to real frequencies $(i\omega_n \to \omega + i0^+)$ gives,

for $\omega << T << \omega_c$

$$\Sigma_R(\omega) \approx \frac{-i\lambda\pi}{2}T + \lambda\omega \log\left(\frac{T}{\omega_c}\right), \tag{B.4}$$

while for $T << \omega << \omega_c$

$$\Sigma_R(\omega) \approx \frac{-i\lambda\pi}{2}\omega + \lambda\omega \log\left(\frac{\omega}{\omega_c}\right). \tag{B.5}$$

These two limiting forms may be combined to reproduce the expression for the self-energy in Eq. 2.2.1.

Bibliography

[1] W.W. Warren,Jr., R.E. Walstedt, G.F. Brennert, G.P. Espinosa and J.P. Remeika, Phys. Rev. Lett. 59, 1860 (1987); P.C. Hammel, M. Takigawa, R.H. Heffner, Z. Fisk and K.C. Ott, Phys. Rev. Lett. 63, 1992 (1989).

[2] G. Grüner, in *Phenomenology and applications of high-temperature superconductors*, editors K.S. Bedell et al., Addison Wesley (1992)

[3] M. Nuss, P.M. Mankiewicz, M.L. O'Malley, E.H. Westerwick, and P.B. Littlewood, Phys. Rev. Lett 63, 3305 (1991); M.L. Horbach and W. van Saarloos, Phys. Rev. B46, 432 (1992).

[4] Z. Schlesinger, R.T. Collins, F. Holtzberg, C. Feild, G. Koren and A. Gupta, Phys. Rev. B41, 11237 (1990); M. Boekholt, M. Hoffmann and G. Güntherodt, Physica C175, 127 (1991); Yonghong Li, Jin Lin Huang and C.M. Lieber, Phys. Rev. Lett. 68, 3240 (1992).

[5] C.M. Varma, P.B. Littlewood, S. Schmitt-Rink, E. Abrahams and A.E. Ruckenstein, Phys. Rev. Lett. 63, 1996 (1989).

[6] D.A. Bonn, P. Dosanjh, R. Liang and W.N. Hardy, Phys. Rev. Lett. 68, 2390 (1992).

[7] P.W. Anderson, in *Frontiers and Borderlines in Many-Particle Physics*, editors R.A. Broglia and J.R. Schrieffer, North-Holland (1988).

[8] Y. Kuroda and C.M. Varma, Phys. Rev. B42, 8619 (1990).

[9] P.B. Littlewood and C.M. Varma, Phys. Rev. B46, 405 (1992); P.B. Littlewood and C.M. Varma, J. Appl. Phys. 69, 4979 (1991).

[10] L.D. Rotter, Z. Schlesinger, R.T. Collins, F. Holtzberg, C. Feild, U.W. Welp, G.W. Crabtree, J.Z. Liu, Y. Fang, K.G. Vandervoort and S. Fleshler, Phys. Rev. Lett. 67, 2741 (1991).

[11] S. Martin, A.T. Fiory, R.M. Fleming, L.F. Schneemeyer and J.V. Waszczak, Phys. Rev. Lett. 60, 2194 (1988).

[12] A.A. Abrikosov, L.P. Gorkov and I.E. Dzyaloshinski, *Methods of quantum field theory in statistical physics*, (Dover Publications, New York, 1975).

[13] R. Akis and J.P. Carbotte, Solid State Comm. 78, 393 (1991).

[14] P.B. Allen and D. Rainer, Nature 349, 396 (1991).

[15] L. Coffey, Phys. Rev. Lett. 64, 1071 (1990).

[16] M. Tinkham, *Introduction to Superconductivity*, (Krieger Publishing Company, Inc., Malabar, 1980).

3 Fluctuation Conductivity and Ginzburg-Landau Parameters in High-Temperature Superconductors above T_c: effect of strong inelastic scattering

3.1 Introduction

The high transition temperature, as well as the short coherence length and the two-dimensionality of the high-T_c cuprate superconductors, enhance the thermal fluctuations of the order parameter near T_c in comparison to classical superconductors. It is therefore of relevance to study the effect of the strong inelastic scattering above the transition temperature on the correction to physical quantities due to these thermal fluctuations.

In this chapter we shall analyze the Azlamasov-Larkin fluctuation conductivity in the presence of the inelastic scattering that leads to the self-energy (Eq. 1.1.1). We will find that this scattering leads to an appreciable change in the Ginzburg-Landau parameters and the current vertex; this in turn leads to a suppression of the fluctuation conductivity as compared to the case of a constant (i.e. independent of frequency, unlike Eq. 1.1.1) pairbreaking scattering rate (e.g. magnetic impurities), which increases with decreasing dimensionality and increasing scattering strength. The suppression is larger the smaller the dimensionality.

It was shown by Ioffe *et al.* [1] that in the c-direction of strongly anisotropic superconductors, fluctuation corrections to the resistivity first lead to a resistivity enhancement, as a consequence of electron scattering against virtual Cooper pairs, before the *zero-dimensional* Azlamasov-Larkin fluctuation correction lowers the resistivity closer to T_c. The magnetic impurity type of pair-breaking, made temperature- but not frequency-dependent, was used in [1], and our findings thus modify those results. We find that their effect is substantially enhanced and might explain the upturn of the c-axis resistivity in the cuprates just above T_c upon lowering the temperature [1].

3.2 Fluctuation conductivity in an MFL above T_c

In the presence of strong pair-breaking the leading contribution to the fluctuation conductivity above the superconducting transition is the Azlamasov-Larkin correction. The Maki-Thompson contribution, which describes the scattering

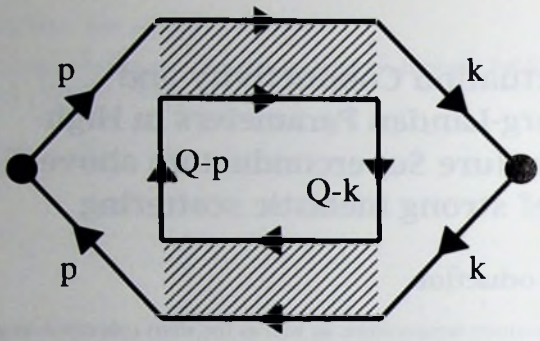

Figure 3-1. The Azlamasov-Larkin contribution to the conductivity. The propagators have a marginal Fermi liquid self-energy and the pair propagator is shown in Fig. 2-1.

of a particle-hole pair into another particle-hole pair by exchange of a virtual Cooper pair, is largely suppressed by the pairbreaking [2]. We shall therefore concentrate on the Azlamasov-Larkin correction for a system which displays marginal Fermi liquid behavior above the superconducting transition.

The Azlamasov-Larkin diagram (Fig. 3-1) represents a contribution to the current

$$j_{AL}(i\Omega_l) = \frac{4e^2}{m^2} T \sum_{i\Omega_m} \int \frac{dQ}{(2\pi)^D} V(Q, i\Omega_m, i\Omega_l)^2 \Gamma(Q, i\Omega_m)\Gamma(Q, i\Omega_m - i\Omega_l) A(i\Omega_l) \tag{3.2.1}$$

where A is the vector potential. The "vertex function" V is given by

$$V(Q, i\Omega_m, i\Omega_l) = -2T \sum_{i\omega_n} \int \frac{dp}{(2\pi)^D} \times$$
$$\times 2pG(p, i\omega_n)G(p, i\Omega_l + i\omega_n)G(Q - p, i\Omega_m - i\Omega_l - i\omega_n) \tag{3.2.2}$$

and $\Gamma(Q, i\Omega_m)$ is the pair propagator.

3.2.1 Calculation of the pair propagator

First, we calculate the pair propagator $\Gamma(Q, i\Omega_m)$. It is given by the sum of the geometric series (Fig. 3-2), $\Gamma = -V/(1 - X)$, where V is the usual BCS model-interaction, which is constant and attractive up to an energy ω_0, and X is given by

$$X(Q, i\Omega_m) = VT \sum_{|\omega_n|<\omega_0} \int \frac{dk}{(2\pi)^D} G(k + Q, i\omega_n + i\Omega_m)G(-k, -i\omega_n) \tag{3.2.3}$$

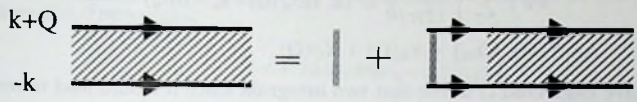

Figure 3-2. The pair propagator $\Gamma(\mathbf{Q}, i\Omega_m)$. The grey lines denote simple BCS interactions, the propagators have a marginal Fermi liquid self-energy (See also Fig. 2-1).

and the temperature Green function in the normal state is

$$G(\mathbf{k}, i\omega_n) = [i\omega_n - \epsilon(\mathbf{k}) - \Sigma(i\omega_n)]^{-1}. \tag{3.2.4}$$

From analytic continuation of the self-energy $\Sigma(\omega)$ it follows (see appendix B) that at the Matsubara frequencies

$$\Sigma(i\omega_n) = -i\lambda\Gamma \arctan\left(\frac{T}{\omega_n}\right) - \frac{1}{2}i\lambda\omega_n \log\left(\frac{\omega_n^2 + \omega_c^2}{\omega_n^2 + T^2}\right). \tag{3.2.5}$$

Here ω_c is an upper cut-off, estimated to be at least 0.5 eV.

We thus consider, as we did in the previous chapter, a system in which the *dominant* interaction leads to marginal Fermi liquid behavior. This does not rule out that a different, weaker interaction (V) causes superconductivity, provided retardation effects play a role such that the different interactions operate on different time scales. (A high transition temperature might in such a case be due to a large scale ω_0 or to the presence of a van Hove singularity in the density of states [3].)

It is the simple BCS model-form we assume for V, that makes an explicit calculation of the pair propagator $\Gamma(\mathbf{Q}, i\Omega_m)$, in the limit of small $\mathbf{Q}$ and small Ω, possible. To this end, we expand $G(\mathbf{k}+\mathbf{Q}, i\omega_n + i\Omega_m)$ to order $|\mathbf{Q}|^2$:

$$\begin{aligned} G(\mathbf{k}+\mathbf{Q}, i\omega_n + i\Omega_m) &= G(\mathbf{k}, i\omega_n + i\Omega_m) + \frac{\mathbf{k}\cdot\mathbf{Q}}{m}G^2(\mathbf{k}, i\omega_n + i\Omega_m) \\ &\quad + \frac{Q^2}{2m}G^2(\mathbf{k}, i\omega_n + i\Omega_m) + \frac{(\mathbf{k}\cdot\mathbf{Q})^2}{m^2}G^3(\mathbf{k}, i\omega_n + i\Omega_m). \end{aligned} \tag{3.2.6}$$

Substitution in the expression for $X(\mathbf{Q}, i\Omega_m)$ gives three terms:

$$\begin{aligned} X(\mathbf{Q}, i\Omega_m) &= VT\sum_{i\omega_n}\int \frac{d\mathbf{k}}{(2\pi)^D} G(\mathbf{k}, i\omega_n + i\Omega_m)G(-\mathbf{k}, -i\omega_n) \\ &\quad + VT\sum_{i\omega_n}\int \frac{d\mathbf{k}}{(2\pi)^D} G^2(\mathbf{k}, i\omega_n)G(-\mathbf{k}, -i\omega_n)\left(\frac{\mathbf{k}\cdot\mathbf{Q}}{m} + \frac{Q^2}{2m}\right) \end{aligned} \tag{3.2.7}$$

$$+VT\sum_{i\omega_n}\int\frac{d\mathbf{k}}{(2\pi)^D}G^3(\mathbf{k},i\omega_n)G(-\mathbf{k},-i\omega_n)\frac{(\mathbf{k}\cdot\mathbf{Q})^2}{m^2}$$
$$\equiv X_A(\mathbf{Q},i\Omega_m)+X_B(\mathbf{Q})+X_C(\mathbf{Q}),$$

where we have neglected Ω in the last two integrals since it would lead to terms of third and higher order smallness.
The first term, $X_A(\mathbf{Q},i\Omega_m)$, gives $\mathcal{N}_0V\log(\frac{2\gamma\omega_D}{\pi T})-\mathcal{N}_0V\frac{\pi\Omega_m}{8T}$. We can expand this to first order in $(T-T_c)$ to obtain:

$$X_A(\mathbf{Q},i\Omega_m) = \mathcal{N}_0V\log\left(\frac{2\gamma\omega_D}{\pi T_c}\right)-\frac{\mathcal{N}_0V}{T_c}(T-T_c)-\mathcal{N}_0V\frac{\pi\Omega_m}{8T_c} \quad (3.2.8)$$
$$= 1-\mathcal{N}_0V\frac{T-T_c}{T_c}-\mathcal{N}_0V\frac{\pi\Omega_m}{8T_c}.$$

The second term, $X_B(\mathbf{Q})$, gives zero: the $\mathbf{k}\cdot\mathbf{Q}$ term gives zero because of $\mathbf{k}\to-\mathbf{k}$ antisymmetry, while the Q^2 term gives zero because the integral over an odd number of propagators is zero.

The third term gives:

$$X_C(\mathbf{Q}) = VT\sum_{i\omega_n}\int\frac{d\mathbf{k}}{(2\pi)^D}\frac{(\mathbf{k}\cdot\mathbf{Q})^2}{m^2}G^3(\mathbf{k},i\omega_n)G(-\mathbf{k},-i\omega_n) \quad (3.2.9)$$
$$= \frac{1}{D}Q^2v_F^2\mathcal{N}_0VT\sum_{i\omega_n}\int d\epsilon_{\mathbf{k}}\frac{1}{\left(i\omega_n-\epsilon_{\mathbf{k}}+\frac{i}{2\tau}\right)^3}\frac{-1}{i\omega_n+\epsilon_{\mathbf{k}}+\frac{i}{2\tau}}$$
$$= \mathcal{N}_0V\frac{v_F^2Q^2}{32D\pi^2T^2}\psi''\left(\frac{1}{2}+\frac{1}{4\pi T\tau}\right).$$

It is possible to rewrite ψ'', the second derivative of the Digamma function $\psi(z)$ with respect to its argument, using

$$\psi(\tfrac{1}{2}+\rho)=\psi(\tfrac{1}{2})+\rho\psi'(\tfrac{1}{2})+\tfrac{1}{2}\rho^2\psi''(\tfrac{1}{2}+\rho)+\mathcal{O}(\rho^3). \quad (3.2.10)$$

After analytic continuation, this finally gives us for the Cooperon:

$$\Gamma_R^{(4)}(\mathbf{Q},z)=-\frac{\mathcal{N}_0^{-1}}{\frac{T-T_c}{T_c}+\eta Q^2-\frac{i\pi z}{8T_c}}, \quad (3.2.11)$$

where η has the form:

$$\eta=-\frac{1}{D}v_F^2\left\{\tau^2\left[\psi(\tfrac{1}{2}+\frac{1}{4\pi T_c\tau})-\psi(\tfrac{1}{2})\right]-\frac{\tau}{4\pi T_c}\psi'(\tfrac{1}{2})\right\}. \quad (3.2.12)$$

In the limiting case $\lambda=0$ one finds the well-known result

$$\Gamma^{-1}(\mathbf{Q},i\Omega_m)=-\mathcal{N}_0\left[\eta Q^2+\alpha\Omega_m+\frac{T-T_c^0}{T_c^0}\right], \quad (3.2.13)$$

where T_c^0 is the usual BCS transition temperature, defined as the temperature where $\Gamma(0,0)$ diverges:

$$T_c^0 = 1.13\omega_0 \exp\left(-\frac{1}{N(0)V}\right) \tag{3.2.14}$$

and where the coefficients η may be obtained from Eq. 3.2.12 with $\tau \to \infty$

$$\eta = \frac{7\xi(3)v_F^2}{16D\pi^2(T_c^0)^2} \tag{3.2.15}$$

and $\alpha = \pi/8T_c^0$.

In the presence of scattering, e.g. as implied by Eq. 3.2.5 or in the presence of impurities, the form of Eq. 3.2.13 for Γ^{-1} is preserved, though the Ginzburg-Landau parameters α and η are renormalized.

It is instructive to first consider the interesting case of magnetic impurity scattering, with a constant scattering rate $1/\tau$ in the Green function G. The suppression of the transition temperature due to the pairbreaking by the magnetic impurities is found to be [4]

$$\ln\left(\frac{T_c^0}{T_c^R}\right) = \psi\left(\frac{1}{2} + \frac{1}{4\pi T_c^R \tau}\right) - \psi\left(\frac{1}{2}\right), \tag{3.2.16}$$

The renormalized Ginzburg-Landau coefficient, which we will denote by η^R, is given by Eq. 3.2.12 with Tc^R substituted for T_c [5]

$$\eta^R = -\frac{1}{D}v_F^2\left\{\tau^2\left[\psi(\frac{1}{2} + \frac{1}{4\pi T_c^R\tau}) - \psi(\frac{1}{2})\right] - \frac{\tau}{4\pi T_c^R}\psi'(\frac{1}{2})\right\}. \tag{3.2.17}$$

This expression is plotted as the dashed curve in Fig. 3-3.

The coefficient α is only slightly modified by the impurity scattering

$$\alpha^R = \frac{\pi}{8T_c^R} + \frac{\psi''(1/2)}{(4\pi T_c^R)^2\tau}. \tag{3.2.18}$$

In the limit of large τ the above expressions reduce to the unrenormalized coefficients.

In presence of the MFL self-energy, Eq. 1.1.1, the renormalized coefficients η^{MFL} and α^{MFL} and the suppressed transition temperature cannot be calculated analytically due to the complicated summation over the Matsubara frequencies in Eq. 3.2.3. The solid curves in figure 3-3 show the result of a numerical evaluation of η^{MFL} as a function of the scattering strength λ, with ω_c/T_c as a parameter. It is seen that η^{MFL} is a decreasing function of λ, and for fixed λ the value of η^{MFL} decreases with increasing ω_c/T_c. It is clear that the marginal Fermi liquid self-energy leads to a reduced value of η, compared to the case of a constant scattering rate. Later we shall see what consequences this has for the Azlamasov-Larkin dc-fluctuation correction.

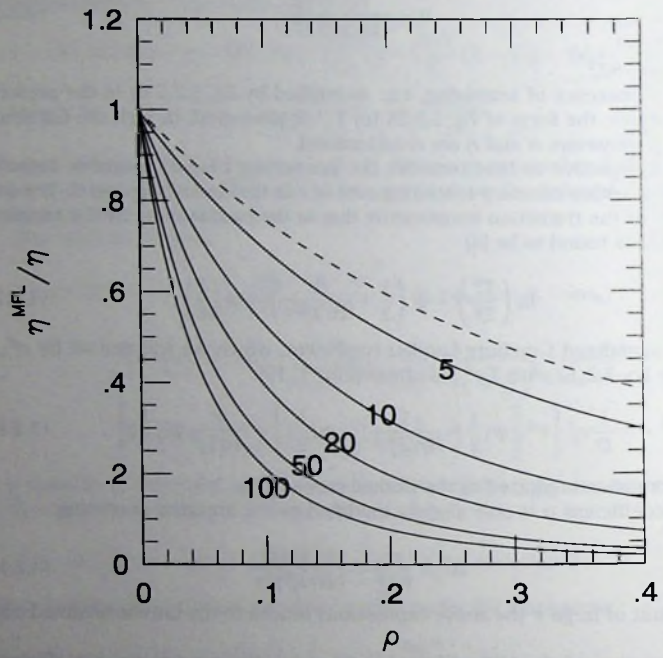

Figure 3-3. The ratio η^R/η (dashed curve) and η^{MFL}/η (solid curves) for the case with a marginal Fermi liquid self-energy (solid curves) with ω_c/T_c as a parameter, both as a function of $\rho = 1/(4\pi T\tau)$. For the marginal Fermi liquid case, with $1/2\tau = \mathrm{Im}\Sigma$ and $T > T_c > \omega = 0$, $\rho = \lambda/4$.

The renormalization of α (Fig. 3-4) expresses how the Ginzburg-Landau relaxation time is renormalized by the inelastic scattering. Of course, the Ginzburg-Landau time is reduced as a result of the pairbreaking by the inelastic scattering. This is of importance for dynamic responses above T_c, but, as we shall see, it also influences the dc-limit. Likewise, the fact that η^{MFL} is reduced relative to η^R, implies a decrease in the correlation length above T_c.

3.2.2 Calculation of the vertex V

The second ingredient that is needed in the calculation of the fluctuation conductivity is the vertex function $\mathbf{V}(\mathbf{Q}, i\Omega_m, i\Omega_l)$, as given in Eq. 3.2.2. We shall calculate only the dc-limit of the conductivity, i.e. the case $\Omega_l = 0$. $\mathbf{V}(\mathbf{Q}, i\Omega_m)$ is evaluated in lowest nonvanishing order in frequency and momentum since the pair propagator is strongly peaked at small values of its arguments and thus $\mathbf{V}$ contributes only significantly at small frequency and momentum.

The expression for the vertex is:

$$\mathbf{V} = -2T \sum_{i\omega_n} \int \frac{d\mathbf{p}}{(2\pi)^D} 2\mathbf{p} G^2(\mathbf{p}, i\omega_n) G(\mathbf{Q} - \mathbf{p}, -i\omega_n)\,, \tag{3.2.19}$$

in D dimensions. Expanding $G(\mathbf{Q} - \mathbf{p}, -i\omega_n)$ for small $|\mathbf{Q}|$:

$$G(\mathbf{Q} - \mathbf{p}, -i\omega_n) \approx G(-\mathbf{p}, -i\omega_n)\left[1 - G(-\mathbf{p}, -i\omega_n)\frac{\mathbf{Q}\cdot\mathbf{p}}{m}\right], \tag{3.2.20}$$

gives $\mathbf{V} = C\mathbf{Q}$, where C is given by

$$C = \frac{4T}{Dm} \sum_{i\omega_n} \int \frac{d\mathbf{p}}{(2\pi)^D} |\mathbf{p}|^2 G^2(\mathbf{p}, i\omega_n) G^2(-\mathbf{p}, -i\omega_n)\,. \tag{3.2.21}$$

In the last step, use has been made of the fact that the first term in the expansion gives zero when substituted in Eq. 3.2.19, because it involves an integral that is antisymmetric in p.

Use has also been made of the identity

$$\int d\mathbf{k}\, \mathbf{k}\mathbf{k} f(|\mathbf{k}|) = \frac{\mathbf{1}}{D} \int d\mathbf{k} |\mathbf{k}|^2 f(|\mathbf{k}|)\,, \tag{3.2.22}$$

where $\mathbf{1}$ is the D-dimensional unit tensor.
Going over from a momentum integration to an energy integration, by using the density of states at the Fermi level, $\mathcal{N}_0$, allows us to obtain

$$C = \frac{4T\mathcal{N}_0 p_F^2}{Dm} \sum_{i\omega_n} \int d\epsilon_{\mathbf{p}} \frac{1}{\left[i\omega_n - \epsilon_{\mathbf{p}} + \frac{i}{2\tau}\mathrm{sgn}(\omega_n)\right]^2} \times \\ \times \frac{1}{\left[-i\omega_n - \epsilon_{\mathbf{p}} - \frac{i}{2\tau}\mathrm{sgn}(\omega_n)\right]^2} \tag{3.2.23}$$

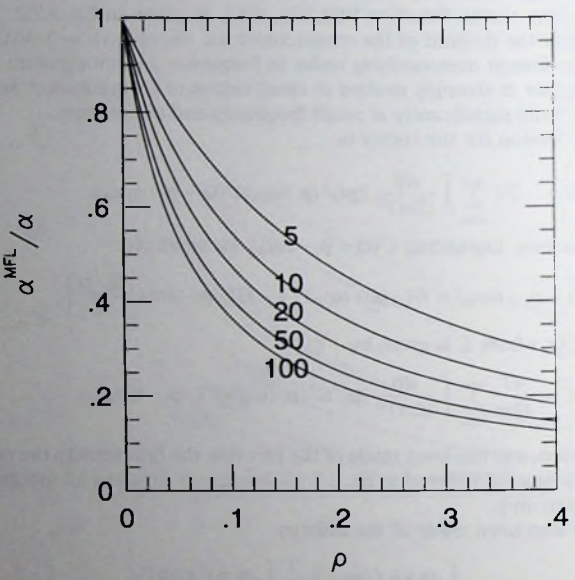

Figure 3-4. Renormalization of the parameter α, normalized to the bare value $\pi/(8T_c)$, as a function of the scattering strength ρ and with ω_c/T_c as a parameter.

$$= \frac{4\pi T \mathcal{N}_0 p_F^2}{Dm} \frac{1}{(2\pi T)^3} \sum_{n=0}^{\infty} \frac{1}{(n+\frac{1}{2}+\frac{1}{4\pi T\tau})^3}$$

Since

$$\sum_{n=0}^{\infty} \frac{1}{(n+\frac{1}{2}+\frac{1}{4\pi T\tau})^3} = -\frac{1}{2}\psi''(\frac{1}{2}+\frac{1}{4\pi T\tau}), \tag{3.2.24}$$

it is possible, using Eq. 3.2.10, to write

$$C = -\frac{\mathcal{N}_0 p_F^2}{2D\pi^2 m T^2}(4\pi T\tau)\left[4\pi T\tau\psi(\frac{1}{2}+\frac{1}{4\pi T\tau}) - 4\pi T\tau\psi(\frac{1}{2}) - \psi'(\frac{1}{2})\right]$$

$$= -\frac{2\mathcal{N}_0 p_F^2}{D\pi m T}\tau\left[4\pi T\tau\psi(\frac{1}{2}+\frac{1}{4\pi T\tau}) - 4\pi T\tau\psi(\frac{1}{2}) - \psi'(\frac{1}{2})\right]. \tag{3.2.25}$$

From Eq. 3.2.25 and Eq. 3.2.12 it is seen that there exists a simple relation between C and η

$$C = 8m\mathcal{N}_0\eta. \tag{3.2.26}$$

3.2.3 The dc fluctuation conductivity

Upon substitution of the expressions we obtained for the vertex $\mathbf{V} = C\mathbf{Q}$ (Eqs. 3.2.19 - 3.2.25) and the Cooperon propagator $\Gamma^{(4)}(\mathbf{Q}, i\Omega_m)$ (Eq. 3.2.11), Eq. 3.2.1 for the current becomes

$$\mathbf{j}_\omega = 4\frac{e^2}{m^2}C^2 T \sum_{i\Omega_m}\int \frac{d\mathbf{Q}}{(2\pi)^D}\mathbf{Q}\mathbf{Q}\frac{\mathcal{N}_0^{-1}}{\left(\frac{T-T_c}{T_c}+\eta Q^2+\frac{\pi\Omega_m}{8T_c}\right)}\frac{\mathcal{N}_0^{-1}}{\left(\frac{T-T_c}{T_c}+\eta Q^2+\frac{\pi\Omega_m+\pi i\omega}{8T_c}\right)}\mathbf{A}_\omega. \tag{3.2.27}$$

Expanding the second fraction with respect to ω, the term linear in ω gives

$$\mathbf{j}_\omega = -i\omega\frac{4e^2}{Dm^2}T_c\frac{\pi}{8T_c}\mathcal{N}_0^{-2}C^2\int\frac{d\mathbf{Q}}{(2\pi)^D}Q^2\sum_{i\Omega_m}\frac{1}{\left(\frac{T-T_c}{T_c}+\eta Q^2+\frac{\pi\Omega_m}{8T_c}\right)^3}\mathbf{A}_\omega. \tag{3.2.28}$$

The sum in this expression may be evaluated as

$$\sum_{m=-\infty}^{\infty}\frac{1}{\left(\frac{T-T_c}{T_c}+\eta Q^2+\frac{\pi\Omega_m}{8T_c}\right)^3} = \frac{-32}{\pi^6}\left[\psi''(\frac{\frac{T-T_c}{T_c}+\eta Q^2}{\pi^2/4}) - \psi''(-\frac{\frac{T-T_c}{T_c}+\eta Q^2}{\pi^2/4})\right] - \frac{1}{(\tau+\eta Q^2)^3}. \tag{3.2.29}$$

By twice differentiating the identity

$$\psi(z) - \psi(-z) = -\pi\cot(\pi z) - \frac{1}{z}, \tag{3.2.30}$$

one sees that the expression in square brackets vanishes linearly for small argument, so that only the last term survives. Thus

$$\mathbf{j}_\omega = i\omega \frac{\pi e^2 C^2}{2Dm^2 \mathcal{N}_0^2} \int \frac{dQ}{(2\pi)^D} \frac{Q^2}{\left(\frac{T-T_c}{T_c} + \eta Q^2\right)^3} \mathbf{A}_\omega . \tag{3.2.31}$$

With Eq. 3.2.26 and the fact that $\mathbf{j} = i\omega\sigma\mathbf{A}$, we finally obtain the expression for the Azlamasov-Larkin correction to the dc-conductivity [9] as

$$\sigma_{AL} = \frac{2^8 e^2 T_c}{D} \alpha\eta^2 \int \frac{dQ}{(2\pi)^D} \frac{Q^2}{\left(\frac{T-T_c}{T_c} + \eta Q^2\right)^3} , \tag{3.2.32}$$

where T_c, η, and α are the renormalized parameters. This expression can also be written as

$$\sigma_{AL} = B_D \alpha \eta^{1-D/2} \left(\frac{T_c}{T - T_c}\right)^{2-D/2} , \tag{3.2.33}$$

where

$$B_D = \frac{2^8 e^2 k_B T_c}{\hbar D} \int_0^\infty dx \frac{x^{D+1}}{(x^2+1)^3} . \tag{3.2.34}$$

In the latter equation, we have reintroduced $\hbar$ and k_B explicitly, so as to make the result for σ_{AL} independent of the units used. As Eq. 3.2.33 shows, the scattering rate dependence enters σ_{AL} through the coefficient $\alpha\eta^{1-D/2}$, and thus has a dimensionality dependent influence.

3.3 Discussion

We have seen that the use of Green functions with the marginal Fermi liquid self energy in the calculation of the dc-Azlamasov-Larkin fluctuation conductivity leads to a change of the parameters η and α, which appear in the final result, Eq. 3.2.33, as the prefactor $\alpha\eta^{1-D/2}$.

In figure 3-5 we have plotted the enhancement factor of the Azlamasov-Larkin contribution due to the marginal Fermi liquid effects in D=3, 2, 1, and 0 compared to the case of a constant magnetic impurity scattering rate as a function of $\rho = 1/(4\pi T_c \tau)$. For the case of the marginal Fermi liquid self-energy above T_c, $1/\tau = \lambda\pi T/2$, $\rho = \lambda/4$. It is seen that the frequency dependence of the pairbreaking scattering rate enhances the effect of the pairbreaking and thus further reduces the fluctuation conductivity. From resistivity measurements it can be estimated that λ varies roughly between 0.25 and 1 in the different cuprates.

Despite the reduction of the fluctuation conductivity, fluctuation effects are observable up to high temperatures due to the small bare conductivity σ_0. The resistance ratio

$$\frac{R}{R_0} = \frac{1}{1 + \sigma_{AL}/\sigma_0} \tag{3.3.1}$$

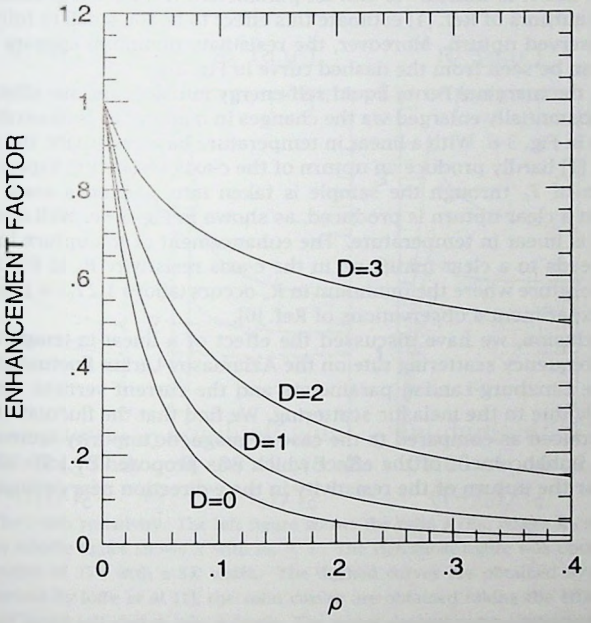

Figure 3-5. The enhancement factor $\left(\frac{\alpha^{MFL}}{\alpha^{x}}\right)\left(\frac{\eta^{MFL}}{\eta^{x}}\right)^{1-D/2}$ of the Azlamasov-Larkin contribution due to the marginal Fermi liquid effects in D=3, 2, 1, and 0 compared to the case of a constant scattering rate as a function of $\rho = 1/(4\pi T\tau)$.

deviates over a large temperature range from 1 when σ_0 is small.

A few years ago, Ioffe *et al.* [1] have shown that in strongly anisotropic materials fluctuation effects initially lead to an increase of the c-axis resistivity above T_c upon lowering the temperature, as a consequence of electron scattering against Cooper pairs, before it drops to zero. The decrease of the conductivity near T_c is first driven by *zero-dimensional* fluctuations and even closer to T_c by three-dimensional fluctuations. This observation might help to understand the observed upturn of the c-axis resistivity near T_c in the cuprate superconductors [6]. While it is difficult to extract parameters from the experiments accurately, the authors of Ref. [1] estimate this effect to be too small to fully account for the observed upturn. Moreover, the resistivity minimum appears too close to T_c, as can be seen from the dashed curve in Fig. 3-6.

Taking the marginal Fermi liquid self-energy into account, the effect by Ioffe *et al.* is substantially enlarged via the changes in η and α, as is illustrated by the solid lines in Fig. 3-6. With a linear in temperature bare resistivity, the results of Ioffe *et al.* [1] hardly produce an upturn of the c-axis resistivity. Especially when a variation of T_c through the sample is taken into account a small shoulder rather than a clear upturn is produced, as shown in Fig. 3-6c. Well above T_c the resistivity is linear in temperature. The enhancement of the upturn in R_c/R_0 in Fig. 3-6a leads to a clear minimum in the c-axis resistivity R_c in Fig 3-6b. The high temperature where the minimum in R_c occurs (above $1.2T_c$) is in agreement with the experimental observations of Ref. [6].

In conclusion, we have discussed the effect of a linear-in-temperature and linear-in-frequency scattering rate on the Azlamasov-Larkin fluctuation conductivity. The Ginzburg-Landau parameters and the current vertices renormalize appreciably due to the inelastic scattering. We find that the fluctuation conductivity is reduced as compared to the case of magnetic impurity scattering. This causes an enhancement of the effect which was proposed by Ioffe *et al.* [1] to account for the upturn of the resistivity in the c-direction near optimal doping.

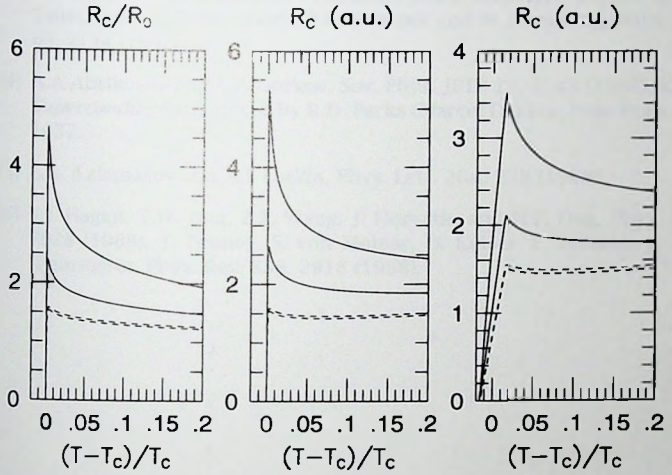

Figure 3-6. The c-axis resistivity. The left figure shows the ratio R/R_0, where R_0 is the bare resistivity, the middle figure shows R with $R_0 \propto T$. The rightmost figure was obtained with a box distribution of T_c's with a $3K$ width. The dashed curves are obtained by using the expression derived by Ioffe *et al.* [1], the solid curves are obtained taking the effects of the marginal Fermi liquid self-energy into account. The upper dashed curve corresponds to λ = 0.6 and the lower dashed curve to λ = 0.3. The same parameters are used for the solid curves.

Bibliography

[1] L.B. Ioffe, A.I. Larkin, A.A. Varlamov and L.Yu, Phys. Rev. B47, 8936 (1993).

[2] J. Keller and V. Korenman, Phys. Rev. B5, 4367 (1972).

[3] J. Labbé and J. Bok, Europhys. Lett. 3, 1225 (1987), D.M. Newns, C.C. Tsuei, P.C. Pattnaik and C.L. Kane, Comments Cond. Mat. Phys. 15, 273 (1992), C.C. Tsuei, C.C. Chi, D.M. Newns, P.C. Pattnaik and M. Däumling, Phys. Rev. Lett. 69, 2134 (1992).

[4] A.A Abrikosov and L.P. Gorkov, Sov. Phys. JETP 12, 1243 (1961); K. Maki, in *Superconductivity*, edited by R.D. Parks (Marcel Dekker, New York, 1969), p. 1037.

[5] L.G. Azlamasov and A.I. Larkin, Phys. Lett. 26A, 238 (1968).

[6] S.J. Hagen, T.W. Jing, Z.Z. Wang, J. Horvath, and N.P. Ong, Phys. Rev. B37, 7928 (1988), T. Penney, S. von Molnár, D. Kaiser, F. Holtzberg, and A.W. Kleinsasser, Phys. Rev. B38, 2918 (1988).

4 The Su–Schrieffer–Heeger model for finite chains

4.1 Introduction

The Su-Schrieffer-Heeger (SSH) Hamiltonian has proven to be a successful theoretical framework for understanding conjugated polymer chains [1-5]. In this tight-binding model one focuses on the coupling between the π-electrons that constitute the valence band, and the ionic motions along the one-dimensional polymeric chain. As is well known, this model exhibits a rich variety of nonlinear phenomena and topological excitations coupling the two possible and equivalent configurations of bond-length alternation in the Peierls distorted ground state.

One motivation for studying this model was presented in the introductory chapter of this thesis. There it was argued that a model, in this spirit, could be a suitable starting point for unraveling the conformational dynamics in the first step in vision. Before we can turn our attention to the dynamics of the untwisting of retinal in chapter 5, it is necessary to formulate more precisely how to study chains of finite length within the framework of an SSH-type model. It is this issue which is the subject of this chapter.

In order to study chains of finite length without the commonly used periodic boundary conditions, the question arises as to which boundary condition to use, *e.g.* whether to leave the chain ends open, or to use a potential at the outer ends to regulate the chain length. Although this question has arisen before, it has, to our knowledge, not been addressed systematically. We will do so in this chapter, and in particular we calculate the value of the stretching force which facilitates comparison between long chains with nonperiodic boundary conditions and those with periodic boundary conditions.

As will become clear below, the prominent part played by the energy-per-site in the model, allows us to obtain a non-perturbative expression for the velocity of sound. Our result shows, that the presence of a finite electron-phonon coupling strength λ reduces the velocity of sound compared to the case where this coupling is absent. For small coupling strengths, however, the reduction is only exponentially small. This observation invalidates perturbative calculations by previous authors.

In section 4.2 we present the SSH model, discuss the boundary conditions and show which choice of a stretching force is most convenient to compare various boundary conditions. We then derive, both heuristically and formally, the aforementioned renormalisation of the sound velocity in section 4.3. In section

4.4 we briefly discuss the generation and subsequent dynamics of kink-antikink pairs on finite chains, and compare it to the the case of these excitations on a chain of infinite length or periodic chains. Finally, in section 4.5, we summarize our findings.

4.2 Model Hamiltonian for finite chains

The one-dimensional tight-binding Hamiltonian we use to describe the physics of the conjugated polymer *trans*-polyacetylene $(CH)_N$, is given by

$$H = H_{el} + H_l\,, \tag{4.2.1}$$

with the π-electron-lattice coupling written as

$$H_{el} = -\sum_{s}\sum_{n=1}^{N-1}\left[t - \alpha(u_{n+1} - u_n)\right]\left[c^{\dagger}_{n,s}c_{n+1,s} + \text{h.c.}\right], \tag{4.2.2}$$

and a lattice part

$$H_l = \frac{K}{2}\sum_{n=1}^{N-1}(u_{n+1} - u_n)^2 + \frac{M}{2}\sum_{n=1}^{N}\dot{u}_n^2 - \Gamma\sum_{n=1}^{N-1}(u_{n+1} - u_n)\,. \tag{4.2.3}$$

In Eqs. (4.2.2) and (4.2.3), n numbers the (CH)-groups, u_n is the displacement along the chain of the n^{th} (CH)-group relative to some reference position na, $c^{\dagger}_{n,s}(c_{n,s})$ creates (annihilates) an electron with spin projection s at site n. The model parameters are: the hopping parameter t for uniform spacing a between adjacent (CH)-groups, the electron-phonon coupling constant α, the force constant K for bond length deviations from equal spacing of the σ-bonding backbone and the mass of a (CH)-group M. The harmonic stretching force Γ will be discussed below.

The π-electron-lattice part of the Hamiltonian H_{el} models the coupling of the π-electrons to the lattice degrees-of-freedom via a linear (distance) modulation of the bare hopping frequency t. The first term in the lattice part of the Hamiltonian H_l models a harmonic restoring force on the σ-bonded (CH)-groups when displaced from equal spacing a, and the second term is the kinetic energy. Up to the last term in Eq. (4.2.3) the three equations constitute the familiar SSH Hamiltonian [1,2].

The last term in Eq. (4.2.3) gives a constant stretching force Γ on a finite chain. As $\sum_{n=1}^{N-1}(u_{n+1} - u_n) = (u_N - u_1)$ denotes the change of length of the chain, it corresponds to a potential term which is linear in the total chain length. Usually, the SSH model is studied with periodic boundary conditions, as these are most convenient to model long, essentially infinite chains. As already recognized by Vanderbilt and Mele [14] and by Su [15], however, for finite *open* chains which

are our interest here, the electronic energy decreases with an overall contraction of the chain due to the linear coupling term proportional to α in H_{el}. Following these authors, a constant stretching force Γ is introduced in the Hamiltonian to counterbalance this compression. With this procedure, one can use the same parameters t, K, and α as in the model with periodic boundary conditions. Note that for periodic boundary conditions this term automatically vanishes, since then $(u_N - u_1) = 0$.

At this point, we note that for finite chains without periodic boundary conditions, two types of boundary conditions have been used: so-called "pressure boundary conditions" with $\Gamma \neq 0$, and "open boundary conditions" with $\Gamma = 0$ [16]. It is important to realize, however, that from the point of view of using the SSH model Hamiltonian as an effective model, both cases describe the same physics: the "pressure boundary conditions" can be transformed into "open boundary conditions" by a redefinition of the variables $\{u_n\}$ and the parameters t and Γ. Indeed, under the uniform stretching transformation $\bar{u}_n = u_n - n\Gamma/K$, we find from Eqs. (4.2.1) and (4.2.3) that to within a constant term

$$H(\{u_n\}; t, K, \Gamma) = H(\{\bar{u}_n\}; t - \alpha\Gamma/K, K, 0)\,. \tag{4.2.4}$$

Hence, contrary to what is sometimes suggested in the literature [16], the dynamics of a chain with pressure boundary conditions is completely equivalent to that of a chain with open boundary conditions, provided we use the renormalized hopping frequency $\bar{t} = t - \alpha\Gamma/K$ and uniformly scaled coordinates [15]. The practical advantage of using the pressure boundary condition with $\Gamma \neq 0$, however, is that with a proper choice of Γ, we may use the same parameter sets and lattice spacing as those used in the literature for periodic chains. These sets were obtained by comparison with experimental data on polyacetylene.

Following Vanderbilt and Mele [14], the value $\Gamma = 4\alpha/\pi$ has often been used in the literature. This is the value derived assuming the ground state is *undimerized*, but in practice a somewhat different value for Γ must be used to obtain the proper dimerized ground state. For small coupling, when the changes in the electronic energies due to the dimerization are exponentially small, the correction to $\Gamma = 4\alpha/\pi$ is also exponentially small.

In this section, we shall determine the value of Γ self-consistently for the dimerized ground state of long chains; as we shall see, for the standard parameter sets, the corrections are non-negligible. In addition, the analysis given below will allow us to determine the ground state energy-per-site $\varepsilon(u, \delta)$ as a function of the uniform dimerization amplitude u and the uniform bond stretching δ. In section 4.3 we show that the optical frequency and sound velocity can be expressed simply in terms of derivatives of $\varepsilon(u, \delta)$. This yields a physically transparent and technically efficient way of calculating the sound velocity exactly [13].

To obtain the approximate ground state we take u_n to be of the form

$$u_n = (-1)^n u - \left(\frac{N}{2} - n\right)\delta\,, \tag{4.2.5}$$

where N is the total number of (CH)-groups. On substitution of Eq. (4.2.5) and neglecting non-extensive terms, the Hamiltonian Eq. (4.2.1) becomes [17]

$$H(u,\delta) = -\sum_{n,s}\left[t + 2\alpha(-1)^n u - \alpha\delta\right]\left[c^\dagger_{n,s}c_{n+1,s} + \text{h.c.}\right] + 2NKu^2 + \frac{1}{2}NK\delta^2 - N\Gamma\delta\,. \tag{4.2.6}$$

The diagonalization of Eq. (4.2.6) can be done in analogy with the usual case of periodic boundary conditions [3], so we will only give some of the essential steps. Since we neglect end effects, our results give the dominant term for Γ and $\varepsilon(u,\delta)$ in the limit $N \to \infty$.

For $\alpha = 0$, $H(u,\delta)$ can be brought to diagonal form by the Bloch operators $c_{ks} = N^{-\frac{1}{2}}\sum e^{-ikna}c_{ns}$ in the extended zone $-\pi < ka < \pi$. For $\alpha \neq 0$, when the dimerization doubles the unit cell, it is convenient to fold the zone into the half zone $-\pi/2 < ka < \pi/2$, with valence $(-)$ and conduction $(+)$ band operators defined as

$$c_{ks-} = \frac{1}{\sqrt{N}}\sum_n e^{-ikna}c_{ns}\,, \tag{4.2.7a}$$

$$c_{ks+} = \frac{-i}{\sqrt{N}}\sum_n e^{-ikna}(-1)^n c_{ns}\,. \tag{4.2.7b}$$

In terms of these operators the Hamiltonian is written as

$$H(u,\delta) = \sum_{ks}\left[\epsilon_k(c^\dagger_{ks+}c_{ks+} - c^\dagger_{ks-}c_{ks-}) + \Delta_k(c^\dagger_{ks+}c_{ks-} + c^\dagger_{ks-}c_{ks+})\right] + 2NKu^2 + \frac{1}{2}NK\delta^2 - N\Gamma\delta\,, \tag{4.2.8}$$

with the energy gap parameter $\Delta_k = 4\alpha u\sin(ka)$ and unperturbed band energy in the reduced zone defined by

$$\epsilon_k = 2(t - \alpha\delta)\cos(ka)\,. \tag{4.2.9}$$

Finally, H is diagonalized by the transformations $a_{ks-} = \beta_k c_{ks-} - \gamma_k c_{ks+}$, and $a_{ks+} = \beta_k c_{ks-} + \gamma_k c_{ks+}$, whose inverses, on substitution in Eq. (4.2.8) give

$$H(u,\delta) = \sum_{ks}E_k(n_{ks+} - n_{ks-}) + 2NKu^2 + \frac{1}{2}NK\delta^2 - N\Gamma\delta\,, \tag{4.2.10}$$

with the quasi-particle energy of the familiar form: $E_k = \sqrt{\epsilon_k^2 + \Delta_k^2}$ and $n_{ks\pm} = a^\dagger_{ks\pm}a_{ks\pm}$. Note that since the ϵ_k and hence E_k depend on the bond stretching δ according to Eq. (4.2.9), the first term of the right-hand-side of Eq. (4.2.10) depends on δ as well.

For the half-filled band of $(CH)_N$, the energy-per-site $\varepsilon(u,\delta)$ for a given dimerization amplitude u and stretch δ is obtained by setting $n_{ks-} = 1$ and $n_{ks+} = 0$ in Eq. (4.2.10), and replacing the sum by an integral:

$$\begin{aligned}\varepsilon(u,\delta) &= \frac{-2}{\pi}\int_0^{\pi/2} E_k\, d(ka) + 2Ku^2 + \frac{1}{2}K\delta^2 - \Gamma\delta \\ &= \frac{-4(t-\alpha\delta)}{\pi}\mathcal{E}(\sqrt{1-z^2}) + 2Ku^2 + \frac{1}{2}K\delta^2 - \Gamma\delta\,,\end{aligned} \tag{4.2.11}$$

where we have introduced the dimensionless variable z, given by

$$z = \frac{2\alpha u}{t-\alpha\delta}\,, \tag{4.2.12}$$

and where $\mathcal{E}$ is the complete elliptic function of the second kind:

$$\mathcal{E}(\sqrt{1-z^2}) = \int_0^{\frac{\pi}{2}} \sqrt{1-(1-z^2)\sin^2(\phi)}\, d\phi\,. \tag{4.2.13}$$

From Eq. (4.2.11) we can determine the ground state dimerization amplitude and uniform stretch for our chains by minimization of the energy. Taking first derivatives with respect to u and δ yields

$$\frac{\partial\varepsilon(u,\delta)}{\partial u} = \frac{8\alpha}{\pi}\frac{z}{1-z^2}[\mathcal{E}-\mathcal{K}] + 4Ku\,, \tag{4.2.14}$$

$$\frac{\partial\varepsilon(u,\delta)}{\partial\delta} = \frac{4\alpha}{\pi}\frac{1}{1-z^2}\left[\mathcal{E}-z^2\mathcal{K}\right] + K\delta - \Gamma\,, \tag{4.2.15}$$

where $\mathcal{K}$ is the complete elliptic integral of the first kind,

$$\mathcal{K}(\sqrt{1-z^2}) = \int_0^{\frac{\pi}{2}} \frac{1}{\sqrt{1-(1-z^2)\sin^2(\phi)}}\, d\phi\,, \tag{4.2.16}$$

and where we have begun to abbreviate $\mathcal{E}(\sqrt{1-z^2})$ and $\mathcal{K}(\sqrt{1-z^2})$ as $\mathcal{E}$ and $\mathcal{K}$.

By differentiating Eqs. (4.2.14) and (4.2.15) once more, we get for the second derivatives of ε with respect to u and δ:

$$\varepsilon_{uu} = \frac{16\alpha^2}{\pi(t-\alpha\delta)}\frac{2\mathcal{E}-(1+z^2)\mathcal{K}}{(1-z^2)^2} + 4K\,, \tag{4.2.17}$$

$$\varepsilon_{\delta\delta} = \frac{4\alpha^2 z^2}{\pi(t-\alpha\delta)}\frac{2\mathcal{E}-(1+z^2)\mathcal{K}}{(1-z^2)^2} + K\,, \tag{4.2.18}$$

$$\varepsilon_{u\delta} = \frac{8\alpha^2 z}{\pi(t-\alpha\delta)}\frac{2\mathcal{E}-(1+z^2)\mathcal{K}}{(1-z^2)^2}\,. \tag{4.2.19}$$

As we will see below, when we discuss the velocity of sound in our model, together with Eq. (4.3.9), these equations give the explicit expressions for the sound velocity.

The ground state configuration can now be determined by setting the first derivatives Eqs. (4.2.14) and (4.2.15) to zero and solving for $\underline{u}$ and $\underline{\delta}$ as a function of the model parameters. It is convenient to introduce a dimensionless electron-lattice coupling strength λ, which is defined here as [18]

$$\lambda = \frac{2\alpha^2}{\pi K t}. \tag{4.2.20}$$

For the stretch per bond $\underline{\delta}$ in the ground state and the parameter z defined in Eq. (4.2.12), we obtain from Eqs. (4.2.14) and (4.2.15) the two coupled equations

$$\frac{\pi K}{4\alpha}\underline{\delta} = \frac{1}{2\lambda} + \frac{\mathcal{E} - \mathcal{K}}{1 - z^2}, \tag{4.2.21a}$$

$$\frac{1}{2\lambda} = \frac{\pi\Gamma}{4\alpha} - \frac{2\mathcal{E} - (1 + z^2)\mathcal{K}}{1 - z^2}. \tag{4.2.21b}$$

These coupled equations can be solved numerically, *i.e.* given Γ and λ one determines z from Eq. (4.2.21b), thus giving the (scaled) stretch $\pi K\underline{\delta}/4\alpha$ on substitution in Eq. (4.2.21a). Fig. 4-1 shows $\underline{\delta}$ as a function of the coupling strength λ for different values of Γ.

As we mentioned previously, we want to tune the parameter Γ in such a way that there is no stretching ($\underline{\delta} = 0$) in the ground state, as in the case of periodic boundary conditions. This value of Γ, where no stretching occurs, is obtained by solving the set of coupled equations

$$\frac{1}{2\lambda} = \frac{\mathcal{K} - \mathcal{E}}{1 - z^2}, \tag{4.2.22a}$$

$$\Gamma_{\delta=0} = \frac{4\alpha}{\pi}\frac{\mathcal{E} - z^2\mathcal{K}}{1 - z^2}. \tag{4.2.22b}$$

Fig. 4-2 depicts the dependence of $\pi\Gamma_{\delta=0}/4\alpha$ on the coupling strength λ. The weak coupling correction to $\Gamma_\delta = 0$ is only exponentially small; for small λ, we obtain from Eqs. (4.2.22a)

$$z \approx 4e^{-(1+1/(2\lambda))}, \tag{4.2.23a}$$

$$\frac{\pi\Gamma_\delta = 0}{4\alpha} \approx 1 - 4\left(\frac{1}{\lambda} - 1\right)e^{-(2+1/\lambda)}, \tag{4.2.23b}$$

where use has been made of the fact that for small z:

$$\mathcal{E}(\sqrt{1 - z^2}) \approx 1 + \frac{z^2}{2}\left(\log(\frac{4}{|z|}) - \frac{1}{2}\right). \tag{4.2.24}$$

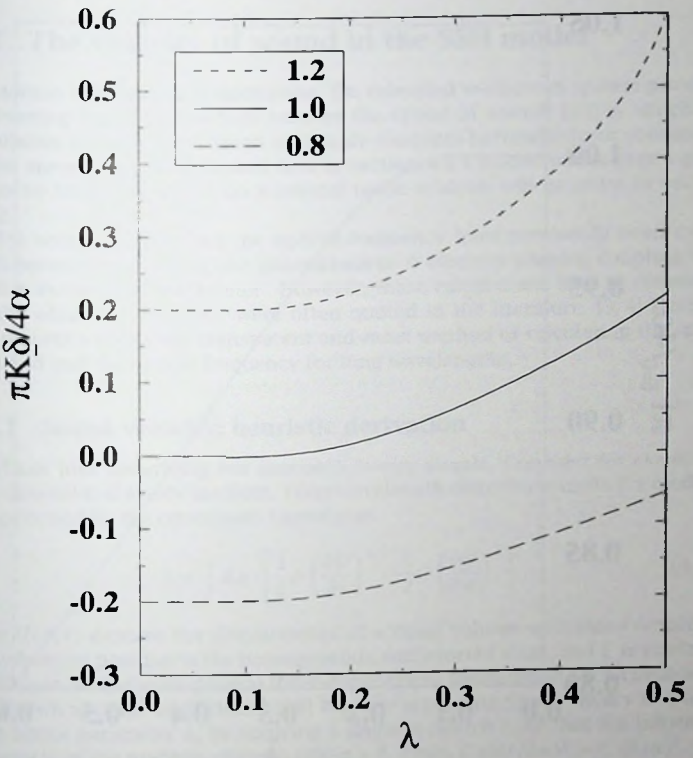

Figure 4-1. The uniform stretch per bond δ as a function of coupling strength λ, for $\Gamma/(4\alpha/\pi) = 0.8$, 1.0, and 1.2.

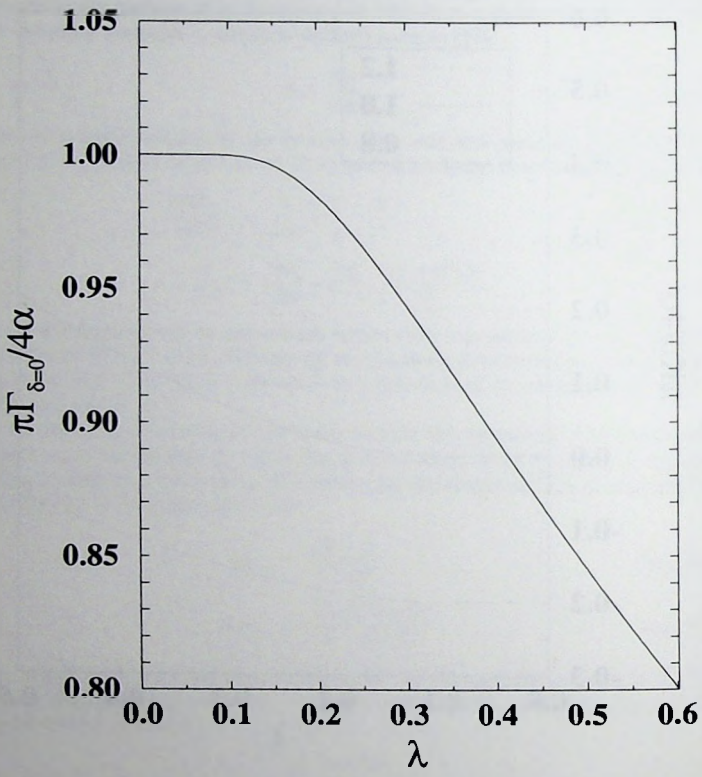

Figure 4-2. Value of Γ that renders $\delta = 0$ in the ground state versus coupling strength λ.

The actual values of the parameters for polyacetylene depend on the type of experiment from which they are extracted [11]. For the different parameter sets used the literature, however, λ lies in the range between 0.2 and 0.4, so that the correction is non-negligible.

4.3 The velocity of sound in the SSH model

In addition to including dimerization, the extended π-electron system provides a screening mechanism which reduces the speed of sound. [23] A simplified calculation of this effect, based on simple concepts borrowed from continuum elastic theory, will be discussed first in section 4.3.1 below, whereafter a more elaborate treatment based on a normal mode analysis will be given in section 4.3.2.

The sound velocity and the optical frequency have previously been calculated perturbatively using the dimensionless π-electron–phonon coupling constant λ as the small parameter. However, these calculations lead to erroneous results which subsequently were often quoted in the literature. [3, 4] Here we will present a physically transparent and *exact* method of calculating the speed of sound and the optical frequency for long wavelengths.

4.3.1 Sound velocity; heuristic derivation

The basic idea underlying our approach is very simple. Consider for example a one-dimensional elastic medium. Long wavelength distortions in such a medium are governed by the continuum Lagrangian

$$L = \int dx \left[\frac{1}{2}\rho \left(\frac{\partial U}{\partial t} \right)^2 - \frac{1}{2} C \left(\frac{\partial U}{\partial x} \right)^2 \right]. \tag{4.3.1}$$

Here $U(x, t)$ denotes the displacement of a small volume with mass density ρ, away from its position in the homogeneous, undistorted state, and C is an elastic coefficient. In the more general three-dimensional formulation such coefficients are known as Lamé coefficients. [24] We now apply this elastic theory to a solid with lattice parameter a, by applying a *uniform stretch* δ, so that the lattice parameter a of the medium changes into $a + \delta$. Thus, $C\,(\partial U/\partial x)^2 = C\,(\delta/a)^2$. The second term in Eq. (4.3.1) then is nothing more than the second-order change in energy density of the medium in the presence of a uniform stretch. In terms of the energy per lattice site ε we therefore have

$$C = a\varepsilon_{\delta\delta}\,, \tag{4.3.2}$$

where $\varepsilon_{\delta\delta}$ denotes the second derivative of ε with respect to a uniform stretch δ. Since the wave equation associated with Eq. (4.3.1) is $\rho\,(\partial^2 U/\partial t^2) = C\,(\partial^2 U/\partial x^2)$,

we immediately have for the speed of sound c

$$c = \sqrt{\frac{C}{\rho}} = a\sqrt{\frac{\varepsilon_{\delta\delta}}{M}}, \tag{4.3.3}$$

where $M = a\rho$ is the mass per lattice site. That it is not necessary to study finite wavevector q oscillations and then take the limit $q \to 0$ to calculate the speed of sound, can be understood as follows. Uniform stretch is in fact the $q = 0$ mode when positions are expressed in *relative* coordinates.

The analysis below is based on the observation that, as was demonstrated in the previous sections, the energy density ε, as a function of the stretch parameter δ, can rather easily be calculated non-perturbatively. Combined with Eq. (4.3.2) this immediately gives the sound velocity. The only complication in applying this idea lies in the fact that as a result of the electron-phonon interaction, changes in the stretch δ are accompanied by changes in the dimerization amplitude u. The exact generalization of Eq. (4.3.2) to this more general case is given below in Eq. (4.3.9), and is based on the fact that the optical frequencies are much higher than the acoustical frequencies for long wavelengths, so that it is permissible to average over the fast optical modes in deriving the effective elastic energy as a function of the stretch δ.

Indeed, due to the arbitrarily large difference in the frequency of acoustic (δ) versus optical (u) modes in the $q \to 0$ limit, we may approximate

$$\overline{\left.\frac{\partial\varepsilon(u,\delta)}{\partial u}\right|_{u=\underline{u}}} = 0, \tag{4.3.4}$$

where the overbar indicates a time average on a time scale short compared to acoustical periods but long compared to optical periods. Put differently, the forces in the optical modes average to zero on acoustic time scales. We can obtain an expression for the value of the time averaged $\overline{\Delta u}$ for a given quasi-static stretch $\Delta\delta$, by expanding Eq. (4.3.4):

$$\varepsilon_{uu}\overline{\Delta u} + \varepsilon_{u\delta}\Delta\delta = 0, \tag{4.3.5}$$

so that the optical modes fluctuate about

$$\overline{\Delta u} = -(\varepsilon_{u\delta}/\varepsilon_{uu})\Delta\delta, \tag{4.3.6}$$

for a given stretch $\Delta\delta$. Expanding the energy-per-site $\varepsilon(u,\delta)$ about the equilibrium values ($\underline{u}$, $\underline{\delta} = 0$) to second order, we have

$$\Delta\varepsilon(u,\delta) = \frac{1}{2}\varepsilon_{uu}(\Delta u)^2 + \varepsilon_{u\delta}(\Delta u)(\Delta\delta) + \frac{1}{2}\varepsilon_{\delta\delta}(\Delta\delta)^2, \tag{4.3.7}$$

where $\Delta\varepsilon(u,\delta) \equiv \varepsilon(u,\delta) - \varepsilon(\underline{u},\underline{\delta})$, $\Delta u \equiv u - \underline{u}$ etc.

Using Eq. 4.3.6 we thus arrive at an expansion for the effective energy with respect to the stretch $\Delta\delta$, valid on acoustic timescales

$$\Delta\varepsilon = \frac{1}{2}\left(\varepsilon_{\delta\delta} - \frac{\varepsilon_{u\delta}^2}{\varepsilon_{uu}}\right)(\Delta\delta)^2 . \tag{4.3.8}$$

In analogy with Eq. 4.3.2, we therefore obtain for the speed of sound in the dimerized ground state

$$c = c_0\sqrt{\frac{\varepsilon_{\delta\delta}}{K} - \frac{\varepsilon_{u\delta}^2}{K\varepsilon_{uu}}}, \tag{4.3.9}$$

where $c_0 = a\sqrt{K/M}$ is the bare speed of sound and where the second derivatives given in Eqs. (4.2.17)-(4.2.19) are to be evaluated at the equilibrium values $\underline{u}$ and $\underline{\delta} = 0$. We stress that, within the adiabatic approximation for the electron dynamics, Eq. (4.3.9) is exact.

Figure 4-3a shows the reduction of the sound velocity as a function of the coupling strength λ. Note that, by expanding the coefficients in Eq. (4.3.9), we find an exponentially small renormalization of the sound velocity for small λ:

$$c/c_0 \approx 1 - 4\left(\frac{1}{\lambda} - 2\right)e^{-(2+1/\lambda)} . \tag{4.3.10}$$

On the one hand, this contradicts the often quoted result [3,4] that the sound velocity for small coupling is given by $c = c_0\sqrt{1-2\lambda}$, and the dashed line in Fig. 4-3a shows this behavior of the sound velocity as obtained by Rice *et al.* [19] On the other hand, Psaltakis and Papanicolaou [26] used a $1/n$ expansion technique for calculating the phonon spectrum, where n is the degeneracy of the π-electron bands ($n = 2$ for polyacetylene), and their result for the suppression of the sound velocity compares extremely well to our exact result.

To illustrate the validity of Eq. (4.3.9), we have also performed numerical simulations in which a sinusoidal modulation was superimposed on the dimerized ground state. The sound velocities were calculated by measuring the resulting periods of oscillations for different λ. As is clear from Fig. 4-3a, where the diamonds represent the simulation results, the agreement with Eq. (4.3.9) is excellent.

It is perhaps not surprising that the effect of the coupling on the sound velocity is only exponentially small in the weak coupling limit, and roughly linear for larger couplings. After all, the effect is a manifestation of the change in chain stiffness which in turn is directly related to the electronic gap. It is well known that the gap is exponentially small in weak coupling, crossing over to linear in λ behavior for larger couplings [3,4].

Since optical frequencies are finite as $q \to 0$, the optical frequency is given in terms of ε_{uu} only: [25]

$$\frac{\omega_{\text{opt}}^2}{\Omega_0^2} = \frac{\varepsilon_{uu}}{4}$$

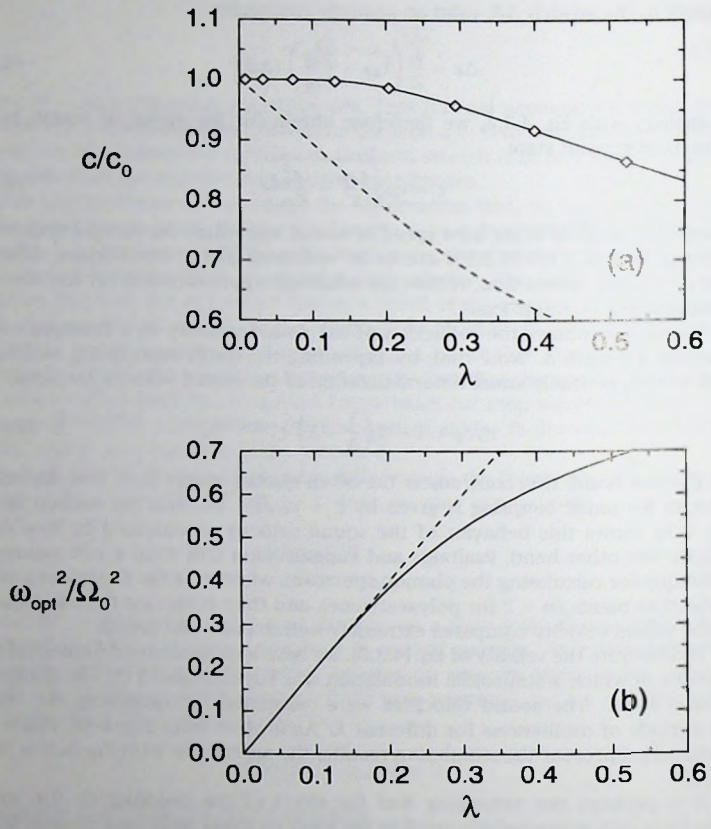

Figure 4-3. (a) Suppression of the sound velocity as a function of the coupling strength λ, defined after Eq. (4.2.19). The solid line shows our analytical result [Eq. (4.3.9)]. The dashed line shows the result obtained by Rice *et al.* [19] The diamonds mark the points we obtained by a numerical simulation (see text), which unambiguously show the validity of our approach. (b) Long wavelength optical frequency as a function of the coupling strength λ. The solid line depicts the exact result [Eq. (4.3.11)]. The dashed line shows the weak-coupling approximation [Eq. (4.3.12)].

$$= 2\lambda \frac{2\mathcal{E} - (1+z^2)\mathcal{K}}{(1-z^2)^2} + 1, \tag{4.3.11}$$

where $\Omega_0 = \sqrt{4K/M}$ is the frequency at the band edge at $\pm\pi/a$ in the absence of dimerization. The solid line in Fig. 4-3b shows the behavior of this optical frequency as a function of λ, while the dashed line depicts the weak coupling result

$$\omega_{\text{opt}} = \sqrt{2\lambda}\,\Omega_0, \tag{4.3.12}$$

obtained from Eq. (4.3.11). Note that, in contrast to the weak coupling behavior [Eq. (4.3.10)] of the sound velocity, our weak coupling result for the optical frequency [Eq. (4.3.12)] and the result given in the literature agree. [3,4,19]

The discrepancy between our exact result for the sound velocity and the result [19] obtained using perturbation theory in λ, can be explained by noting that the weak coupling behavior [Eq. (4.3.10)] shows an essential singularity at $\lambda = 0$. This behavior can therefore never be obtained using perturbation theory in λ. On the other hand, the analytic behavior for small λ of the optical frequency [Eq. (4.3.12)] can be obtained correctly using perturbation theory.

In summary, the method described above presents a technically simple and physically transparent way of obtaining expressions for the sound velocity and optical frequency which can furthermore be applied to other models of the SSH variety. These quantities may serve as a guide to determine the validity of spectra calculated by other means.

4.3.2 Sound velocity; normal mode analysis

Through the physically transparent and relatively simple analysis given in the previous section, we arrived at the exact expression for the sound velocity as a function of the electron-phonon coupling strength λ: Eq. 4.3.9. In this section we show, how this result may also be obtained from a more conventional normal-mode analysis.

As a starting point we take the classical equation of motion for the j^{th} (CH)-group, expressed in external coordinates:

$$M\ddot{x}_j = -\frac{\partial E}{\partial x_j}, \tag{4.3.13}$$

where $E = E(\{x_i\})$ is the total energy which, in the adiabatic approximation, depends on the nuclear coordinates only. Changing to internal coordinates with two atoms per unit cell:

$$\delta_{2n} = \frac{1}{4}(x_{2n+3} + x_{2n+2} - x_{2n+1} - x_{2n}), \tag{4.3.14}$$

$$\nu_{2n} = x_{2n+1} - x_{2n}, \tag{4.3.15}$$

we obtain the two coupled equations of motion

$$-4M\ddot{\delta}_{2n} = -\frac{1}{2}\frac{\partial E}{\partial \delta_{2n-2}} + \frac{\partial E}{\partial \delta_{2n}} - \frac{1}{2}\frac{\partial E}{\partial \delta_{2n+2}}, \tag{4.3.16}$$

$$-M\ddot{v}_{2n} = 2\frac{\partial E}{\partial v_{2n}}. \tag{4.3.17}$$

On introducing the Fourier transforms

$$\tilde{\delta}_q = \frac{2}{N}\sum_{n=1}^{N/2} \delta_{2n} e^{iq(2an)}, \tag{4.3.18}$$

$$\frac{\partial}{\partial \tilde{\delta}_p} = \sum_{n=1}^{N/2} e^{-ip(2an)} \frac{\partial}{\partial \delta_{2n}}, \tag{4.3.19}$$

and expanding around the first derivatives in Eqs. (4.3.16) and (4.3.17), we obtain the equations of motion in the form

$$-M\ddot{\tilde{\delta}}_q = \frac{A(q)}{2N}\sum_p \left[\tilde{\delta}_p \frac{\partial^2 E}{\partial \tilde{\delta}_{-q}\partial \tilde{\delta}_p} + \tilde{v}_p \frac{\partial^2 E}{\partial \tilde{\delta}_{-q}\partial \tilde{v}_p}\right], \tag{4.3.20}$$

$$-M\ddot{\tilde{v}}_q = \frac{4}{N}\sum_p \left[\tilde{\delta}_p \frac{\partial^2 E}{\partial \tilde{v}_{-q}\partial \tilde{\delta}_p} + \tilde{v}_p \frac{\partial^2 E}{\partial \tilde{v}_{-q}\partial \tilde{v}_p}\right], \tag{4.3.21}$$

with $A(q) = 1 - \cos(2qa)$. Defining the energy-per-site $\varepsilon \equiv E/N$, substituting $(-i\omega_q)$ for a time derivative and taking advantage of translational invariance in the ground state, we find

$$M\omega_q^2 \tilde{\delta}_q = \frac{A(q)}{2}\left[\tilde{\delta}_q \frac{\partial^2 \varepsilon}{\partial \tilde{\delta}_{-q}\partial \tilde{\delta}_q} + \tilde{v}_q \frac{\partial^2 \varepsilon}{\partial \tilde{\delta}_{-q}\partial \tilde{v}_q}\right], \tag{4.3.22}$$

$$M\omega_q^2 \tilde{v}_q = 4\left[\tilde{\delta}_q \frac{\partial^2 \varepsilon}{\partial \tilde{v}_{-q}\partial \tilde{\delta}_q} + \tilde{v}_q \frac{\partial^2 \varepsilon}{\partial \tilde{v}_{-q}\partial \tilde{v}_q}\right]. \tag{4.3.23}$$

One final change of coordinates to account for the dimerization amplitude u_{2n} is defined from $v_{2n} = \delta_{2n} + 2u_{2n}$. The derivatives with respect to δ in Eq. 4.3.20 through Eq. 4.3.23 are to be taken with v constant. Since we need to have these derivatives with u constant, we write

$$\left.\frac{\partial}{\partial \tilde{\delta}_{-q}}\right|_v = \left.\frac{\partial}{\partial \tilde{\delta}_{-q}}\right|_u + \left.\frac{\partial \tilde{u}_{-q}}{\partial \tilde{\delta}_{-q}}\right|_v \left.\frac{\partial}{\partial \tilde{u}_{-q}}\right|_\delta$$

$$= \left.\frac{\partial}{\partial \tilde{\delta}_{-q}}\right|_u - \frac{1}{2}\left.\frac{\partial}{\partial \tilde{u}_{-q}}\right|_\delta. \tag{4.3.24}$$

We thus obtain

$$M\omega_q^2 \begin{pmatrix} \tilde{\delta}_q \\ \tilde{v}_q \end{pmatrix} = \begin{pmatrix} \frac{1}{2}A(q)(\bar{\varepsilon}_{\delta\delta} - \bar{\varepsilon}_{u\delta} + \frac{1}{4}\bar{\varepsilon}_{uu}) & \frac{1}{4}A(q)(\bar{\varepsilon}_{\delta u} - \frac{1}{2}\bar{\varepsilon}_{uu}) \\ 2(\bar{\varepsilon}_{u\delta} - \frac{1}{2}\bar{\varepsilon}_{uu}) & \bar{\varepsilon}_{uu} \end{pmatrix} \cdot \begin{pmatrix} \tilde{\delta}_q \\ \tilde{v}_q \end{pmatrix}, \tag{4.3.25}$$

where we have introduced the notation

$$\tilde{\varepsilon}_{xy} \equiv \frac{\partial^2 \varepsilon}{\partial \tilde{x}_{-q} \partial \tilde{y}_q} . \tag{4.3.26}$$

In the long wavelength limit, where $\lim_{q\to 0} \tilde{\varepsilon}_{xy} = \varepsilon_{xy}$, we therefore find for the acoustic frequency

$$\omega = qa \sqrt{\frac{\varepsilon_{\delta\delta} - \varepsilon_{\delta u}^2 / \varepsilon_{uu}}{M}} , \tag{4.3.27}$$

from which we obtain the sound velocity as

$$c = c_0 \sqrt{\frac{\varepsilon_{\delta\delta} - \varepsilon_{\delta u}^2 / \varepsilon_{uu}}{K}} , \tag{4.3.28}$$

with $c_0 = \sqrt{K/M}$, which reproduces Eq. (4.3.9). The $q \to 0$ optical frequency becomes, according to Eq. (4.3.25),

$$\omega_{\text{opt}} = \sqrt{\frac{\varepsilon_{uu}}{M}} . \tag{4.3.29}$$

It is worth stressing again, that within the adiabatic approximation Eqs. (4.3.28) and (4.3.11) are exact. They can be calculated explicitly using Eqs. (4.2.17)—(4.2.19) evaluated at the equilibrium values $\underline{u}$ and $\underline{\delta}$.

The optical frequency can also be explicitly calculated from Eqs. (4.3.29) and (4.2.17). For weak coupling we obtain

$$\omega_{\text{opt}} \approx \sqrt{2\lambda}\, \Omega_0 , \tag{4.3.30}$$

where $\Omega_0 = \sqrt{4K/M}$ would be the ($q = 0$) optical frequency in the absence of π-electron-phonon coupling. This result and that given in the literature agree [13].

4.4 Dynamics

Since, as explained in the introduction, our interest ultimately lies in exploring the dynamical pathway to conformational changes in rhodopsin as it adsorbs a photon, we conclude this chapter by briefly discussing dynamical simulations of photoexcitations for finite chains.

Our chief aim here is to investigate the effect of the stretching force Γ (pressure boundary conditions) on the dynamics of a kink-antikink pair formed when an electron is excited from the top of the valence band into the bottom of the conduction band. In particular, since these solitons are repelled from the ends of a chain [15], one expects that dynamically generated solitons will be reflected by the chain ends. The results presented below confirm this expectation, and show that solitons and breathers [20,21] are still recognizable entities on small chains [10].

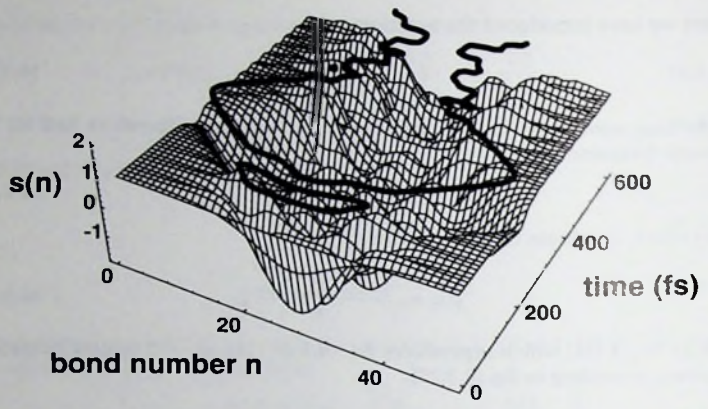

Figure 4-4. The kink-anti-kink dynamics on a $N = 50$ chain, with the parameters given in the text. The heavy line denotes the zero crossings of $s(n)$ and shows how a kink, initially moving towards the chain end with an approximately uniform speed, is reflected on approaching the end at a distance ξ. It moves back again with approximately uniform speed.

Our simulation technique is based on the adiabatic approximation using the Feynman-Hellmann theorem [22]. In short, the procedure is to diagonalize the electronic Hamiltonian at every time step, and to calculate the electronic forces on the (CH) groups using the Feynman-Hellmann theorem.

To illustrate the generic dynamics on an open chain of finite length, we present the results we obtained for a chain of $N = 50$ sites and parameter values set to [20,21]: $t = 2.5$ eV, $\alpha = 4.8$ eV/Å, $K = 17.3$ eV/Å^2 and $M = 1384$ eV fs^2/Å^2. These parameters imply a coupling strength $\lambda = 0.34$ from the definition of λ in Eq. (4.2.20). For the value of $\Gamma_{\delta=0}$, needed to obtain a ground state with zero bondstretch, we find $\Gamma_{\delta=0} = 5.648$ eV/Å from Eqs. (4.2.22a) and (4.2.22b). Furthermore, the electronic length scale ξ , which determines the width of a kink, is found to be $\xi/a = (2t/\Delta) \approx 2.5$.

Fig. 4-4 shows a three-dimensional representation of the dynamics. Along the vertical axis we have plotted the bond elongation relative to its ground state value, i.e. $s(n) \equiv (u_{n+1} - u_n)/(\underline{u}_{n+1} - \underline{u}_n)$. With the heavy line we show the $s(n) = 0$ crossing (shifted upwards for better visibility).

Obviously the dynamics on this open chain very much resembles the dynamics on chains with periodic boundary conditions in the first instants. After about 100 femtoseconds a kink-antikink pair is clearly formed, moving apart with approximately uniform speed (heavy line). As in periodic chains, a spatially localized oscillating mode or "breather" is left behind because, as pointed out

by Bishop *et al.* [20, 21], the energy of the two moving kinks is less than the energy injected by creating the electron-hole pair. The surplus energy is radiated backwards by the moving kink and anti-kink and forms the breather. The kink and anti-kink continue to move apart with approximately uniform velocity, until they are at a distance of the order ξ from the end. There they bounce back because solitons are repelled from the ends [15] and move towards the center, again with an approximately uniform speed. Finally, the kink and anti-kink interact with each other and with the breather in a complicated way; they then re-emerge from this zone after about 600 femtoseconds. Coulomb interaction of the charged kink and anti-kink may be important in understanding the eventual relaxation of the molecule to its final state.

For different parameters the length scales and time scales are of course different, but we have found the dynamics described above to be generic. We leave a more systematic study of finite chain dynamics to the future.

4.5 Summary

We have shown how the introduction of an additional degree of freedom, a uniform bond stretch, enables us to apply the SSH model to finite open chains. The advantage of this approach lies in the fact that one can use the same parameter sets for our finite chains as used for infinite chains with periodic boundary conditions.

Both these results and those for the renormalization of the sound velocity are given in terms of the energy-per-site $\epsilon(u, \delta)$. Our method is, in fact, completely general in that it can be applied to any model in which an effective energy for the long wavelength modes can be written down [13].

The initial (adiabatic) dynamics, following the excitation of an electron from the top of the valence band into the bottom of the conduction band, is qualitatively the same as the dynamics on periodic chains, and confirm that solitons are reflected at the chain ends.

The insights we have obtained in studying the SSH-model on finite chains will help us to move on to a more elaborate model for the conformational changes in rhodopsin after photo-excitation. To this end, torsional degrees-of-freedom and ionic or other site impurities may each play a part. It is our belief that the same classical coherent dynamics as seen in the SSH-model, plays an essential role in the first step of vision, and investigations along these lines will be the subject of the next chapter.

Bibliography

[1] W.P. Su, J.R. Schrieffer and A.J. Heeger, Phys. Rev. Lett. **42**, 1698 (1979).

[2] W.P. Su, J.R. Schrieffer and A.J. Heeger, Phys. Rev. B **22**, 2099 (1980).

[3] A.J. Heeger, S. Kivelson, J.R. Schrieffer and W.P. Su, Rev. Mod. Phys. **60**, 781 (1988).

[4] Yu Lu, *Solitons & Polarons in Conducting Polymers* (World Scientific, Singapore 1988).

[5] D. Baeriswyl, in *Theoretical Aspects of Band Structures and Electronic Properties of Pseudo-One-Dimensional Solids*, ed. H. Kamimura, (Reidel 1985).

[6] W.P. Su and J.R. Schrieffer, Proc. Natl. Acad. Sci. USA **77**, 5626 (1980).

[7] E.J. Mele, Solid State Comm. **44** , 827 (1982).

[8] E.J. Mele, Phys. Rev. B **26**, 6901 (1982).

[9] F. Guinea, Phys. Rev. B **30**, 1884 (1984).

[10] One study of finite molecules is: J.L. Brédas and A.J. Heeger, Chem. Phys. Lett. **154**, 56 (1989). For short molecules in the first electronically excited state, they study the size-dependence of relaxed solitonic steady-states. [See also J.L. Brédas, J.M. Toussaint, and A.J. Heeger, Mol. Cryst. Liq. Cryst. **189**, 81 (1990).]

[11] R.W. Schoenlein, L.A. Peteanu, R.A. Mathies and C.V. Shank, Science **254**, 412 (1991).

[12] H.J.M. de Groot, unpublished.

[13] F.L.J. Vos, D.P. Aalberts and W. van Saarloos, Phys. Rev. **B53**, R5986 (1996).

[14] D. Vanderbilt and E.J. Mele, Phys. Rev. B **22**, 3939 (1980).

[15] W.P. Su, Solid State Comm. **35**, 899 (1980).

[16] S.R. Phillpot, D. Baeriswyl, A.R. Bishop and P.S. Lomdahl, Phys. Rev. B **35**,7533 (1985).

[17] We follow common practice [3] in calling Eqs. (4.2.6) and (4.2.8) Hamiltonians. Strictly speaking, the electronic part is written in the form of a Hamiltonian, but as it does not depend on the individual coordinates of the CH-groups anymore, the lattice part in Eq. (4.2.8) is not a proper Hamiltonian.

[18] Note that there are several conventions for the definition of the coupling strength λ in the literature, mostly differing by factors of two.

[19] M.J. Rice, S.R. Phillpot, A.R. Bishop and D.K. Campbell, Phys. Rev. B 34, 4139, (1986).

[20] A.R. Bishop, D.K. Campbell, P.S. Lomdahl, B. Horovitz and S.R. Phillpot, Phys. Rev. Lett. 52, 671 (1984).

[21] A.R. Bishop, D.K. Campbell, P.S. Lomdahl, B. Horovitz and S.R. Phillpot, Synthetic Metals 9, 223 (1984).

[22] C. Cohen-Tannoudji, B. Diu and F. Laloë in *Quantum Mechanics* Vol.2, p. 1192 (Wiley-Interscience, London 1991).

[23] L. Salem, *Molecular Orbital Theory of Conjugated Systems*. (Benjamin, London, 1966).

[24] See e.g. L.D. Landau and E.M. Lifshitz, *Theory of Elasticity*, (Pergamon, New York, 1986).

[25] F.L.J. Vos, D.P. Aalberts and W. van Saarloos, Phys. Rev. B53, 14922 (1996).

[26] G.C. Psaltakis and N. Papanicolaou, *Phonons and quantum fluctuations in a dimerized electron-phonon chain*, in Interacting Electrons in Reduced Dimensions, ed. D. Baeriswyl and D.K. Campbell, (Plenum Press, New York, 1988).

5 Towards Understanding the Ultra-Fast Dynamics of Rhodopsin

5.1 Introduction

Trying to understand how we see has occupied researchers for more than 100 years [1]. Vision in twilight conditions is attributed to rhodopsin, the complex formed by the chromophore 11-*cis*-retinal bound in the pocket of a rod membrane protein called opsin. In the 1950s, vision was shown to arise from the rapid 11-*cis* to 11-*trans* isomerization of retinal [2]. The cones, responsible for color vision, also rely on the photoisomerization of 11-*cis*-retinal, differing only in the protein cages which surround the chromophore; however, in what follows, we will consider only rhodopsin's photochemistry.

We may be on the verge of understanding why rhodopsin is such an efficient and fast switch. The reason for calling rhodopsin a switch is, that the optically active element, retinal, has two primary conformations—11-*cis* (rhodopsin or Rh) and 11-*trans* (bathorhodopsin or bRh)—and absorption of an optical photon (~ 5000Å) toggles the states. Recent experiments [3] show that, for rhodopsin, the isomerization is accomplished in a mere 200 femtoseconds, about the time it takes light to cross the width of a hair. Vibrational oscillations of the photoproduct cohere for a few ps [4], much longer than the isomerization time. The photoisomerization is also very reliable, with 67% quantum efficiency; that, together with a high stability against thermal fluctuations (400 years), yields the startling signal-to-noise ratio that makes the rod cells of our eyes essentially single photon detectors. The efficiency and speed are believed to be related quantities, in fact, since slower switches are observed to be less efficient [5]. Once a photon has flipped the switch, a sequence of dark reactions—driven thermally—follows, leading eventually to a nerve signal.

In this chapter, we introduce the extension to the SSH model with the aim to analyse the fast dynamics of rhodopsin. The model is still in a testing stage, so this final goal has not been achieved yet. Here we will describe the model, and discuss how insight in the behavior of the model and values for the various parameters appearing in it can be obtained from a calculation of its vibrational modes.

5.2 Previous Theory

Birge and his colleagues [6] did molecular dynamics calculations in the early 1980s and predicted isomerization times of ~ 2.2 ps. While this looks quite long in light of the current measurements with femtosecond lasers, the outcome of their calculation was already quite surprising, as it was believed at that time to be too short for such a large conformational change. Their approach was a one-spatial-degree-of-freedom model: only rotations about the C_{11}=C_{12} bond were considered, holding other relative coordinates fixed. In recent years, they have revised their calculation to include interaction with a counterion and now find it takes the excited state 400 fs to reach the minima of the excited state surface from which it tunnels to bRh or Rh, then ~ 1 ps to cool vibrationally to that local minimum [6]. Experiments indicate an essentially barrierless process [4].

Contemporaneously Su, Schrieffer, and Heeger (SSH) were investigating polyacetylene (PA), another material with double bonds in conjugation, and proposing their celebrated one-dimensional model [7, 8]. As was shown in chapter 4 solitons appear in pairs with astounding rapidity, following photoexcitation. As illustrated in Fig. 5.2b, a soliton is a compact and coherent (long-lived) lattice deformation pattern which smoothly bridges from a double-single to a single-double bonding pattern. Interestingly, solitonic lattice distortions draw energy levels into the gap [9–11]. The conclusion is that the energy surface is sensitively dependent on the vibrating coordinates, not independent of time. Therefore, after photoexcitation, the retinal exits the Franck-Condon regime so quickly in part because forming solitons (in a few fs) reshapes the original energy landscape.

What we are attempting to do is to apply SSH's simple conceptual framework for PA to the more difficult problem of rhodopsin and its non-trivial three-dimensional structure. To fix the parameters of our model, we use measured vibration frequencies and we are aided by recent NMR experiments and *ab initio* calculations which indicate the structure of retinal. One immediate advantage of our approach is that we may study (photo)excited electronic states in a relatively simple and fast way, even on a modest-size workstation. Furthermore, correlation effects may also be included in these calculations in a transparent way; this is not possible in *ab initio* density functional approaches and is perhaps misleading in the approach of [6] because they neglect the effect of other spatial coordinates on the energy surface.

5.3 Model

As in the previous chapter, we will build upon the foundation laid by SSH in modeling the conjugated backbone with a tight-binding Hamiltonian in which the quantum mechanics for independent π electrons is retained explicitly, while the other backbone forces arising from the sp^2 electrons and nuclear repulsion

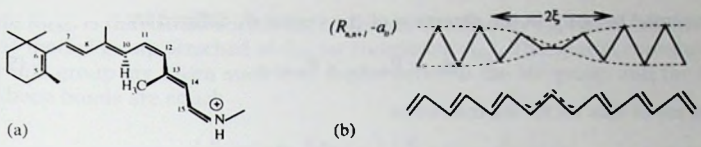

Figure 5-1. (a) 11-*cis*-retinal. (b) A soliton of width 2ξ: bond lengths $R_{n,n+1}$ oscillate about mean value a_0. Below, the same in standard chemical notation. Note that the soliton interchanges the bonding pattern (double-single ↔ single-double).

are treated with springlike effective potentials. Since electrons are much lighter than nuclei, we shall again assume that electrons instantaneously adjust to the wavefunctions that are evolving due to nuclear motion (the adiabatic or Born-Oppenheimer approximation). The essential electron-lattice coupling produces a dimerized lattice (alternating single and double bonds) and opens up a gap in the spectrum due to the Peierls instability. The gap, which determines much of what happens after photoexcitation, and the topological excitations seen in the SSH model, are believed to persist when electron-electron interactions are included [9, 12]. In this chapter we will go beyond SSH in generalizing to a fully three-dimensional model, in explicitly considering finite chains, and in adding steric and electrostatic interactions specific to rhodopsin.

Our primary additional assumption in modeling three-dimensional conjugated polymers is of sp^2p_z hybridization. That is to say that the p_z orbital of a carbon atom is perpendicular to the plane containing the three sp^2 orbitals. Using the Rh ground state coordinates determined in the *ab initio* calculations of Bifone, de Groot, and Buda (BGB) [14], we find near planarity of the sp^2 orbitals, even in the highly sterically strained regions. That gives us some confidence in this idealization.

Even with the simplifications, many elements contribute to our Hamiltonian. These can be explored one by one. The π-electron–lattice coupling is written as

$$H_{el} = -\sum_s \sum_n \left[\left(t - \alpha(R_{n,n+1} - a_0) \right) \cos\theta_{n,n+1} \right] \left[c^\dagger_{n,s} c_{n+1,s} + c^\dagger_{n+1,s} c_{n,s} \right] , \quad (5.3.1)$$

where $a_0 = 1.4$ Å is the average carbon-to-carbon spacing, $R_{i,j} = |\vec{R}_{i,j}| = |\vec{r}_j - \vec{r}_i|$ is the actual bond length between atoms i and j, and the operator $(c^\dagger_{i,s} c_{j,s})$ is the compact second-quantization notation for moving an electron with spin s from site j to site i (with appropriate fermion properties implicit). Our intuition that electrons move more readily when the p_z orbitals are close together is reflected in H_{el} for positive α and t. Twisting the p_z orbitals out of alignment also reduces the likelihood of π-electron hopping [15]. We measure the degree of twisting with θ, the angle between neighboring p_z orbitals. The p_z orbital is always taken to be perpendicular to the adjacent molecular bonds. Thus, the p_z orbital

is assumed to point in the direction of the vector $\vec{\pi}$, defined by

$$\vec{\pi}_n = \vec{R}_{n-1,n} \times \vec{R}_{n,n+1} . \tag{5.3.2}$$

In terms of this vector we may write

$$\cos\theta_{n,n+1} = \frac{-\vec{\pi}_n \cdot \vec{\pi}_{n+1}}{|\vec{\pi}_n||\vec{\pi}_{n+1}|} . \tag{5.3.3}$$

The bond stretching, bond-angle bending, and kinetic terms are all included in the lattice part of the Hamiltonian:

$$\begin{aligned} H_l &= \frac{K_\sigma}{2}\sum_n (R_{n,n+1} - a_0)^2 + \frac{K_{120}}{2}\sum_n (\Delta\phi_n)^2 \\ &\quad + \sum_n \frac{M_n}{2}\dot{\vec{r}}_n^{\,2} - \Gamma\sum_n (R_{n,n+1} - a_0) , \end{aligned} \tag{5.3.4}$$

where M_n is the mass of the (C_nH) or (C_nMe) group at position n, where "Me" stands for a Methyl group ($-CH_3$)) and where, as we saw in chapter 4, Γ is a term which regulates the chain length for finite chains [16]. Since in retinal conjugation begins at C_5, sums begin with $n = 5$. Furthermore, $\Delta\phi_n$ is the deviation in radians of the bond angle from $2\pi/3$ rad = 120°. To first order in this deviation we have

$$\Delta\phi_n \approx \frac{R_{n-1,n+1}^2 - R_{n-1,n}^2 - R_{n,n+1}^2 - R_{n-1,n}R_{n,n+1}}{\sqrt{3}R_{n-1,n}R_{n,n+1}} . \tag{5.3.5}$$

So far, the model is generally applicable to conjugated polyene systems in three dimensions. To study rhodopsin, at least two additional terms must be included. One contribution stems from having a protonated Schiff base (PSB) at one end of the conjugated system. The nitrogen in the PSB is also sp^2p_z hybridized (isoelectronic to carbon), but tends to attract electrons to itself more than a carbon. We may model this simply with an on-site potential

$$H_N = V_N\rho_N, \text{ where } \rho_N = \sum_s c_{N,s}^\dagger c_{N,s} . \tag{5.3.6}$$

This contribution is simply V_N times the electron density ($-e\rho$ is charge density) at site N.

One further contribution to the Rh Hamiltonian is the steric interaction due to the crowding in the crook of the *cis* bond, especially the steric interaction between the methyl group attached to C_{13} and the hydrogen attached to C_{10} (see Fig. 5.2a). Significant distortions result—taking the flat molecule and twisting it out of the plane [14,18]. We model the steric interactions with an r^{-12} potential

$$H_{St} = A\,(R_{\mathrm{H,Me}})^{-12} , \tag{5.3.7}$$

where $R_{H,Me}$ is the distance from the hydrogen attached to C_{10} (at coordinate $\vec{r}_H$) to the methyl group attached to C_{13} (at coordinate $\vec{r}_{Me}$). The spatial coordinates of a side group are taken such that angles between the Me group and the two backbone bonds are equal:

$$\vec{r}_{Me} = \vec{r}_{C_{13}} + a_{CC}\left(\frac{\vec{R}_{C_{13},C_{12}}}{R_{C_{13},C_{12}}} + \frac{\vec{R}_{C_{13},C_{14}}}{R_{C_{13},C_{14}}}\right)\left|\frac{\vec{R}_{C_{13},C_{12}}}{R_{C_{13},C_{12}}} + \frac{\vec{R}_{C_{13},C_{14}}}{R_{C_{13},C_{14}}}\right|^{-1}, \tag{5.3.8}$$

where $a_{CC} = 1.54$Å is the carbon-carbon distance from C_{13} to the carbon atom of the attached methyl group. An expression analogous to Eq. 5.3.8 is used for the hydrogen, with $a_{CH} = 1.1$Å.

The complete Hamiltonian is a sum of these terms:

$$H = H_{el} + H_l + H_N + H_{St}. \tag{5.3.9}$$

The full dynamics of the atomic coordinates is performed by using the Feynman-Hellman theorem to calculate the forces, integrating forward, and recalculating at each step the electronic wavefunctions of the new configuration [16].

Our next challenge is to fix the parameters of the model. We take as our starting point the length over which the dimerization pattern varies in the ground state ξ, related to the dimensionless electron-phonon coupling parameter λ by the asymptotic expression [12]

$$\xi/a_0 \approx \tfrac{1}{4}\exp(\tfrac{1}{2\lambda} + 1), \text{ with } \lambda = \frac{2\alpha^2}{\pi K_\sigma t}. \tag{5.3.10}$$

Fitting to experiments done on PA, SSH found $\xi/a_0 = 7$. From Eq. 5.3.10, we find a relatively small electron-lattice coupling $\lambda = 0.21$. This is the value used in the calculations reported below.

5.4 Structure and Vibrations

We carried out a full analytical vibrational analysis of the *trans*-PA case of our model (chain in the xy-plane extending in the x direction as shown in Fig. 5.4 and $H_{PA} = H_{el}+H_l$), for small electron-phonon coupling. The angular frequencies ω for the acoustical and optical modes are [13]:

$$\begin{aligned}
M\omega^2_{x,ac} &= \frac{32K_\sigma\tilde{K}_{120}}{K_\sigma + 12\tilde{K}_{120}}Q_x^2, & M\omega^2_{x,op} &= 6K_\sigma\lambda, \\
M\omega^2_{y,ac} &= 0Q_y^2 + \tfrac{4}{3}\tilde{K}_{120}Q_y^4, & M\omega^2_{y,op} &= K_\sigma + 12\tilde{K}_{120}, \\
M\omega^2_{z,ac} &= \frac{256t}{3\pi a_0{}^2}Q_z^2, & M\omega^2_{z,op} &= 0,
\end{aligned} \tag{5.4.1}$$

where $\tilde{K}_{120} = K_{120}a_0{}^{-2}$ and $Q_x = q_x\frac{\sqrt{3}a_0}{2}$ is a phase angle. Direct numerical simulation of these vibration modes confirm Eq. 5.4.1. The optical torsional and

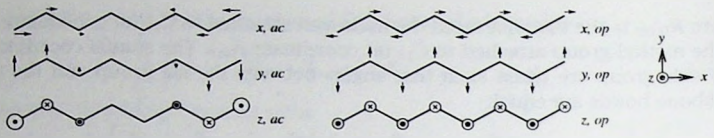

Figure 5-2. Atomic displacement patterns for acoustical and optical modes. The frequency of each mode is given in Eq. 5.4.1.

acoustic bending modes correspond merely to rotations out of the xy plane and in the xy plane, respectively; there is no restoring force for such displacements so they are zero-frequency modes. The calculation for $\omega_{x,op}$ employs an asymptotic expansion in λ for the energy and, as such, is only valid for small λ; the physical value of $\lambda = 0.21$ is small enough that the asymptotic expansion is still good.

Since we are interested in determining the structure of Rh and its vibrational spectra, it is measurements of these quantities which we used to set the remainder of the parameters. Raman spectroscopy studies [19] indicate optical modes of period 30 fs ($\approx$ 1100 cm^{-1}) for x and period 25.8 fs ($\approx$ 1290 cm^{-1}) for y. Optical frequencies differ little between PA or β-carotene. Using the formulae, we find $K_{sigma} = 47$ eV/Å^2 and $K_{120} = 5.6$ eV/(rad)^2. (1 eV = 23 kcal/mol.)

In Fig. 5.2, the acoustical modes are shown as uniform compression, bend, or twist. These deformations vibrate with period given by the slowest mode, the mode with wavelength twice the length of the molecule; thus, $Q_{\min} = \pi/(N-1)$. It is interesting to use these expressions to calculate the frequency of the slowest acoustical mode. The compression mode is fastest with a period of 110 fs. The torsional mode has period $220/\sqrt{t/\text{eV}}$ fs; for reasonable values of t (discussed later) this is the next fastest. The slowest is the bending mode. Because $Q = \pi/11$ yields primarily a rotation, we must look to the mode with $Q = 2\pi/11$. We find this mode has period 385 fs, which compares favorably to the measured period of 550 fs in the bRh photoproduct [4]. Therefore we attribute the vibrational ringing of the photoproduct to the bending, not the twisting mode. This leads to a new way of thinking about the photoisomerization: a quick nonlinear untwisting of the 11-*cis* bond excites many modes, but the observed coherent oscillations will be associated with the lowest frequency provided other frequencies are well separated from it. According to our calculations, this is mostly of bending (y) character.

Different measurements lead to conflicting values of t. Based on the π bandwidth of PA, SSH find $t = 2.5$ eV; however, with this value, steric strain is absorbed by bond-angle bending rather than by twisting—the ground state is flat, in contrast to the BGB structure. On the other end of the scale, values calculated by *ab initio* studies of torsional spring constants around single and double bonds in hexatriene [20] indicate $t \sim 0.4$ eV. This would suggest an optical gap

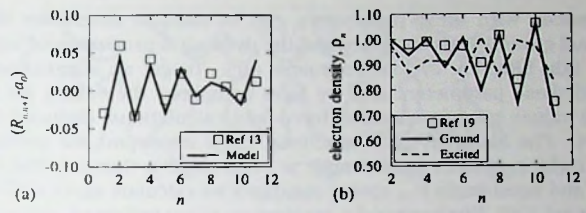

Figure 5-3. (a) Dimerization pattern compared to *ab initio* calculations [14]. Note the solitonic pattern (compare with Fig. 5.1b) centered near $n = 9$. (b) Ground-state electron density compared with NMR measurement [21]. In the photoexcited state, the electron density near the nitrogen increases. Qualitative agreement is good.

an order of magnitude too small. We take, at present, an intermediate value $t = 1$ eV to achieve reasonably good agreement with the BGB structure, and an electronic gap of 0.62 eV. From Eq. 5.3.10 we find $\alpha = 3.94$ eV/Å which, upon using Eq. 4.2.22a, fixes $\Gamma(\alpha, \lambda) = 4.92$ eV/Å.

The BGB ground state shows a solitonic dimerization pattern due to the electron withdrawal from the backbone by the PSB, as can be seen in Fig. 5.3. Far from the nitrogen, bond lengths alternate uniformly. Near the nitrogen, this difference goes to zero—in fact, the formal C_{14}–C_{15} bond really is short and the C_{15}=N bond is long. The constant $V_N = -2.15$ eV produces a bond length alternation pattern consistent with that found by BGB [14] and charge oscillations [21]. The constant $A = 4000$ Å^{12}·eV was chosen to yield the measured spacing between the methyl and carbons 10 and 11:

$$R_{\mathrm{Me},C_{10}} = \begin{cases} 3.04 \text{ Å} & \text{model} \\ 3.05 \pm 0.03 \text{ Å} & \text{(ref [18])} \end{cases}, \tag{5.4.2}$$

and

$$R_{\mathrm{Me},C_{11}} = \begin{cases} 3.10 \text{ Å} & \text{model} \\ 3.05 \pm 0.05 \text{ Å} & \text{(ref [18])} \end{cases}, \tag{5.4.3}$$

and torsional angles consistent with the BGB result:

$$\{\theta_{C_{10},C_{11}}, \theta_{C_{11},C_{12}}, \theta_{C_{12},C_{13}}\} = \begin{cases} \{15°, 169°, 8°\} & \text{model} \\ \{11°, 164°, 14°\} & \text{(ref [14])} \end{cases}. \tag{5.4.4}$$

Other torsional angles are near 0° since no steric interactions are included to twist them. That $\theta_{C_{11},C_{12}}$ is near 180° indicates that it is a *cis* bond (5.3.2). Parameters A and V_N are not yet optimized for a best fit, but qualitative features are achieved.

This model, with these parameters, can be used to determine the three-dimensional ground-state structure and the dynamical properties of conjugated polymers (Rh, bRh, PA, cyclooctatetraene, etc). To get an impression of how reasonable these parameters are, we have compared the values we have derived with values used in chemical force-field calculations, deduced for hexatriene [20]. The hierarchy of interactions, most important for getting global structure right, is correct: bond length $\gg$ bond angle $\gg$ torsion. The compressional K_σ and bond-angle K_{120} spring constants we calculate agree well quantitatively with ref. [20]. Our torsional t constant is, as we indicated above, a couple of times larger than for hexatriene, but fits into the hierarchy.

One might wonder how our calculations differ from atomic force field approaches. The key is that we treat the collective response of the electrons which gives rise to the possibility for solitons, polarons, etc. We may also treat electronically excited states, which is also not possible in force-field calculations.

5.5 Photoexcitation

As we have seen in the previous chapter, where the photoexcitation of finite chains was dicussed, the dimerization pattern interchanges in the center of the molecule persistently [16]. This means that in the center, until vibrational cooling or some other mechanism damps out the kinetic energy, what were double bonds become single bonds, and vice versa. In Fig. 5.4 we demonstrate that this is also the case for Rhodopsin, in particular that the C_{11}=C_{12} bond ($n = 7$) becomes a long bond. We imagine a mechanism in which the creation of soliton pairs (inverting the bond alternation pattern in between) *dynamically catalyzes* the isomerization. The system starts sterically strained; by interchanging single and double bonds, the torsional stiffness at the C_{11}-C_{12} bond is weakened. Without a large barrier, can the steric strain do the job of twisting the molecule to the less sterically strained bathorhodopsin configuration? Our simulations, to date, do not realize this plausible scenario. Possibly, electron-electron interactions of the Hubbard type play an important role in this aspect of the dynamics [22]. The recent developments of the Density Matrix Renormalization Group, which allows the treatment of strong electron-electron interactions in one-dimensional models with unprecedented accuracy, appears to pave the road for the inclusion of such correlations in our model [17].

The charge density along the retinal backbone is another quantity which changes upon photoexcitation of Rh. In the calculations of Birge *et al.* [6] the net charge, near the nitrogen atom, changes by about $0.25e$. This effect is observed in our simulations (see Fig. 5.3).

Here we have ignored interactions of the retinal with the protein. These interactions may assist in the photoisomerization and are cuurently a subject of research by Aalberts and coworkers. Yet within 200 fs, the protein cannot adjust

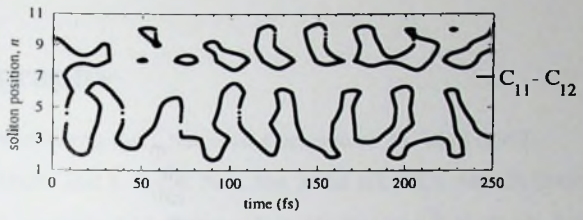

Figure 5-4. The positions of solitons that emerge after photoexcitation (the lines denote the positions where the dimerization pattern changes sign $R_{n,n+1} = R_{C_{n+4},C_{n+5}} = a_0$). Recall Fig. 5.2b. Note that C_{11}=C_{12} bond becomes and remains a single bond after about 10 fs. Steric strain prevents returning to double-bond character in spite of the small conjugation length (N = 12).

much to the conformational change of the retinal, the exception being motion of the lysine residue that binds the retinal to the protein. Protein interactions which may play an important role include: vibrational cooling, holding ring in place, deformation due to the lysine tugging on the end (perhaps related to the energy storage mechanism of bathorodopsin), and the counterion. As long as experiments can fix the additional interaction parameters which need to be added, the modeling can proceed.

Although much work remains to be done, we are optimistic that a model of the type discussed here, will provide the clues to understand rhodopsin's photoisomerization. *Dynamical catalysis* is one such novel mechanism inspired by this approach. The model is also of general utility in studying the three-dimensional structure and intermediates of other systems with π-conjugated backbones.

Bibliography

[1] Reviewed briefly by: J. Nathans. *Biochemistry* **31**, 4923 (1992).

[2] R. Hubbard and A. Kropf. *Proc. Nat. Acad. Sci. U.S.A.* **44**, 130 (1958).

[3] R. W. Schoenlein, L. A. Peteanu, R. A. Mathies, and C. V. Shank. *Science* **254**, 412 (1991).

[4] Q. Wang, R. W. Schoenlein, L. A. Peteanu, R. A. Mathies, and C. V. Shank. *Science* 266, 422 (1994).

[5] R. W. Schoenlein, L. A. Peteanu, Q. Wang, R. A. Mathies, and C. V. Shank. *J. Phys. Chem.* 97, 12 087 (1993).

[6] R.R. Birge and L.M. Hubbard. *J. Am. Chem. Soc.* **102**, 2195 (1980). R.R. Birge and L.M. Hubbard. *Biophys. J.* **34**, 517 (1981). R.R. Birge, C.M. Einterz, H.M. Knapp, and L.P. Murray. *Biophys. J.* **53**, 367 (1988). R.R. Birge. *Annu. Rev. Phys. Chem.* 41, 683 (1990).

[7] W.P. Su, J.R. Schrieffer, and A.J. Heeger. *Phys. Rev. Lett.* **42**, 1698 (1979).

[8] W.P. Su, J.R. Schrieffer, and A.J. Heeger. *Phys. Rev. B* **22**, 2099 (1980).

[9] A.J. Heeger, S. Kivelson, J.R. Schrieffer and W.P. Su. *Rev. Mod. Phys.* **60**, 781 (1988).

[10] Yu Lu, *Solitons & Polarons in Conducting Polymers* (World Scientific, Singapore 1988).

[11] D. Baeriswyl, in *Theoretical Aspects of Band Structures and Electronic Properties of Pseudo-One-Dimensional Solids*, ed. H. Kamimura, (Reidel 1985).

[12] D. Baeriswyl, D.K.Campbell, and S. Mazumdar. In *Conjugated Conducting Polymers*, ed. H.G. Kiess (Springer *Sol. St. Sci.* **102**, 1992).

[13] D. P. Aalberts, F. L. J. Vos and W. van Saarloos, *in preparation.*

[14] A. Bifone, H.J.M. de Groot, and F. Buda, Pure & Appl. Chem., **69**, 2105 (1997), and references therein.

[15] W.A. Harrison. *Electronic Structure and the Properties of Solids* (W.H. Freeman, San Francisco, 1980).

[16] F.L.J. Vos, D.P. Aalberts, and W. van Saarloos, *Phys. Rev. B*, **53** 14 922 (1996).

[17] C. Zhang, E. Jechelmann and S.R. White, cond-mat/9709187 (1997).

[18] P.J.E. Verdegem, P.H.M. Bovee-Geurts, W.J. de Grip, J. Lugtenburg, and H.J.M. de Groot. In preparation.

[19] F. Inagaki, M. Tasumi, and T. Miyazawa. *J. Raman Spect.* 3, 335 (1973).

[20] F. Negri, G. Orlandi, A.M. Brouwer, F.W. Langkilde, and R. Wilbrandt. *J. Chem. Phys.* 90, 5944 (1989).

[21] H.J.M. de Groot. Personal communication.

[22] D. P. Aalberts, *private communication*

Samenvatting

Hieronder geef ik een korte samenvatting van de resultaten van mijn onderzoek zoals die in de vorige hoofdstukken, op meer wetenschappelijke wijze, gepresenteerd zijn.

Het eerste deel van mijn promotie onderzoek, waarvan de resultaten te vinden zijn in hoofdstuk 2 en hoofdstuk 3, heeft betrekking op de fenomenologie van hoge-temperatuur supergeleiding. Om deze resultaten in een juiste context te kunnen plaatsen, zal ik eerst iets algemeens vertellen over supergeleiding.

Supergeleiding werd in 1911 door Kamerlingh Onnes ontdekt, in het natuurkundig laboratorium in Leiden dat thans zijn naam draagt. Hij ontdekte dat wanneer kwik tot beneden zo'n 3 Kelvin (-270°C) wordt afgekoeld, de elektrische weerstand van het kwik plotseling nul wordt. Later werd dit effect ook gevonden bij andere metalen zoals aluminium, tin en lood. De temperatuur waarbeneden de elektrische weerstand nul wordt, wordt de "kritieke temperatuur" genoemd. De toestand waarin het betreffende metaal zich beneden deze temperatuur bevindt de "supergeleidende toestand". Boven de kritieke temperatuur heet het materiaal in de "normale" toestand te zijn; de term "normaal" geeft hierbij aan dat het materiaal zich als een gewoon metaal gedraagt. Behalve deze meest in het oog springende eigenschap, het verdwijnen van de elektrische weerstand, werden in de loop der tijd nog andere fysische eigenschappen van deze materialen gevonden, die optreden in de supergeleidende toestand.

Het duurde echter tot halverwege de vijftiger jaren, voordat een bevredigende theoretische verklaring van het verschijnsel supergeleiding gegeven kon worden door de amerikaanse fysici Bardeen, Cooper en Schrieffer. Hun theorie, nu bekend onder de naam BCS-theorie, verklaarde vanuit een microscopische onderbouwing de vele verschijnselen die bij supergeleiders optreden. Centraal in die onderbouwing staat het concept "gepaarde elektronen". Op het eerste gezicht lijkt het vreemd dat twee elektronen een paar zouden willen vormen, aangezien zij immers een gelijke elektrische lading hebben en elkaar dientengevolge zullen afstoten. BCS toonden echter aan dat beneden een bepaalde temperatuur, m.b.v. in het metaal aanwezige roostertrillingen (fononen), twee elektronen een netto aantrekkingskracht op elkaar kunnen uitoefenen. Omdat dit voor alle elektronen opgaat impliceert dit dat de normale toestand, waarin de elektronen niet gepaard zijn, instabiel is beneden de kritieke temperatuur waardoor bij lager wordende temperatuur meer en meer elektronen met andere elektronen "condenseren" in paren. Dit leidt tot een collectieve toestand met de voor supergeleiders bekende eigenschappen.

Supergeleidende materialen vonden in de loop der tijd allerlei nuttige toepassingen. Om praktische en economische redenen lag het voor de hand om materialen te vinden met een zo hoog mogelijke kritieke temperatuur; de "klassieke" supergeleiders zoals lood en tin hebben een vrij lage kritieke temperatuur en het is dus duur en onpraktisch om ze met vloeibaar helium op die lage temperatuur te brengen en te houden.

In 1987 ontdekten de fysici Bednorz en Müller, dat een nieuwe klasse van keramische materialen supergeleidend wordt bij temperaturen die hoger zijn dan het kookpunt van vloeibaar stikstof, zo'n $-200°C$. Deze materialen, hogetemperatuur supergeleiders, vonden natuurlijk snel hun toepassingen, maar stelden de theoretici opnieuw voor een groot raadsel. Het bleek namelijk dat deze materialen ten opzichte van de klassieke supergeleiders, naast de uitzonderlijk hoge kritieke temperatuur, een aantal eigenschappen hebben die niet passen binnen de BCS-theorie. Hierbij vielen vooral enkele eigenschappen op die deze materialen hebben boven de kritieke temperatuur: de normale toestand van hoge-temperatuur supergeleiders blijkt in die zin abnormaal te zijn. Opnieuw leverden theoretici enorme inspanningen om een microscopische verklaring voor deze eigenschappen te vinden.

Een aantal van deze onverklaarbare en op het eerste gezicht niet samenhangende experimentele feiten werd in 1989 door Varma en collega's in één enkele formule samengevat. Deze auteurs poneerden een fenomenologische theorie, die gebaseerd was op één aanname m.b.t. de polariseerbaarheid van de materialen. Deze Marginal Fermi Liquid (MFL) aanname bleek voldoende in staat om bij het doorrekenen van de consequenties ervan een aantal experimenteel bekende eigenschappen te reproduceren. In deze berekeningen werd aangenomen dat het mechanisme dat verantwoordelijk is voor het MFL gedrag, tevens de "lijm" tussen de elektronen is bij paarvorming (zoals de fononen de "lijm" tussen de elektronen zijn in het geval van klassieke BCS supergeleiders) in de supergeleidende toestand. In hoofdstuk 2 van dit proefschrift, laten we zien dat dit geen noodzakelijke aanname is; door uit te gaan van elektronen die zich als een MFL gedragen èn een afzonderlijk mechanisme voor supergeleiding à là BCS, laten zich door berekening resultaten afleiden die ook consistent zijn met experimenteel bekende eigenschappen, maar die nu wel eenvoudiger begrepen kunnen worden.

In hoofdstuk 3 berekenen we de consequenties van de MFL-aanname voor de geleidbaarheidsfluctuaties in supergeleiders, in de richting loodrecht op de koperoxide vlakken waaruit deze materialen zijn opgebouwd. Uit deze berekeningen blijkt dat de weerstandstoename vlak boven de kritieke temperatuur, zoals die experimenteel wordt waargenomen, ook vanuit de MFL-fenomenologie kan worden verklaard.

Het tweede deel van mijn onderzoek betreft een onderwerp dat ligt tussen

fysica van polymeren en de biologie, en is beschreven in hoofdstuk 4 en hoofdstuk 5.

Als U dit in een zeer schemerig hoekje leest, komen lichtdeeltjes (fotonen) vanaf het witte gedeelte van deze bladzijde op Uw netvlies. In dat netvlies bevinden zich cellen die, vanwege hun vorm, staafjes worden genoemd; deze staafjes gebruiken wij (en andere gewervelden) nu net om in relatieve donkerte te kunnen zien. In het membraan van deze cellen bevinden zich op hun beurt grote eiwitmoleculen, opsine genaamd. Een opsine molecuul heeft zich als een verpakking heeft gesloten rond een veel kleiner molecuul: retinal. De combinatie van het eiwit opsine met daarin het kleine retinal molecuul, dat overigens in zekere zin een door midden geknipt β-caroteen molecuul is dat vooral in de bekende wortels voorkomt, wordt rhodopsine genoemd.

Het retinal molecuul bevindt zich niet zomaar in het eiwit, maar heeft een zeer specifieke gebogen vorm die de *cis* vorm wordt genoemd. Wanneer echter een foton dit cis-retinal treft, veroorzaakt dit een vormverandering van het gebogen (cis) naar een recht (trans) retinal molecuul. Dit rechte retinal past nu echter niet meer zo goed in het opsine molecuul en begint van binnenuit te wrikken, waardoor een reeks stappen in gang wordt gezet die leidt tot een zenuwimpuls naar de hersenen: we zien!

Van de meeste van de hierboven genoemde stappen in het mechanisme van het zien, is sinds kortere of langere tijd veel bekend. De meest essentiële stap echter, de eerste stap, waarbij cis-retinal omvormt naar trans-retinal werpt zeker vanuit theoretisch standpunt interessante vragen op, die tot nu toe onbeantwoord zijn gebleven. De uitdaging is namelijk, te verklaren waarom deze fotochemische reactie zich in slechts zo'n 200 femtoseconde kan afspelen. Zelfs voor fotochemische begrippen is deze tijd namelijk zeer kort (ter illustratie, 200 femtoseconde oftewel 0.0000000000002 seconde, is de extreem korte tijd die licht ongeveer nodig heeft om de afstand van één haardikte af te leggen...). Een andere vraag is, waarom deze reactie zo efficient is: lichtintensiteiten die overeenkomen met een paar fotonen zijn met het blote, weliswaar aan het donker gewende, oog waarneembaar!

Nu is retinal in essentie een geconjugeerd molecuul, wat wil zeggen dat het een keten van koolstofatomen bevat, waarin dubbele ("korte") chemische bindingen en enkelvoudige ("lange") chemische bindingen elkaar afwisselen. Op de eindige lengte en wat interessante zijgroepen na, lijkt retinal daarom veel op een bekend polymeer: polyacetyleen. Dit molecuul is in het verleden onderwerp van veel theoretisch-fysisch onerzoek geweest, en een model voor dit molecuul werd gegeven door de fysici Su, Schrieffer en Heeger: het SSH-model. Dit model, waarin de quantummechanische eigenschappen van alleen de valentie-elektronen (die elektronen die bij de chemische binding betrokken zijn) worden inbegrepen voorspelt, voor redelijke waarden van de parameters in het model, effecten op tijdschalen die veel overeen lijken te komen met de tijdschaal van 200 femtoseconde bij de eerste stap in het zien, en die daarbij mogelijk een rol zouden

kunnen spelen.

In hoofdstuk 4 nemen we daarom het SSH-model als uitgangspunt. De resultaten in dit hoofdstuk zijn primair bedoeld om inzicht te krijgen in de eigenschappen van het model bij de toepassing ervan op ketens met een eindige lengte. Wat dan blijkt is, dat het SSH-model met een geringe aanpassing geschikt is om ook eindige ketens te beschrijven. Een aardig bijprodukt van de analyse is een exacte formule voor de geluidssnelheid; hieruit blijkt dat resultaten op dit gebied die vroeger met benaderende methoden werden verkregen niet juist zijn.

In hoofdstuk 5 breiden we het model zodanig uit, dat beweging van het molecuul in meer richtingen is toegestaan. Dit is van essentieel belang om de cis-trans overgang van retinal te kunnen modelleren. Bij deze uitbreiding van het model worden enkele nieuwe parameters geïntroduceerd. Om realistische waarden voor deze parameters te bepalen, worden de frequenties van mogelijke trillingen (normal modes) uitgerekend. Door deze frequenties te vergelijken met experimenteel bekende waarden, kunnen de waarden van de parameters van het model bepaald worden.

Hoewel deze resultaten nog niet leiden tot uitspraken over retinal en de eerste stap in het zien, is het werk dat in dit hoofdstuk beschreven staat wel een belangrijke en noodzakelijke eerste stap om, in een later stadium van dit onderzoek, de ultra-snelle dynamica van rhodopsine te gaan begrijpen.

List of publications

- *Phenomenology of the superconducting state of a marginal Fermi liquid with BCS model-interaction*, M. L. Horbach, F. L. J. Vos, and W. van Saarloos, Physical Review B48, 4061 (1993) [Chapter 2].
- *Fluctuation conductivity and Ginzburg-Landau parameters in high-temperature superconductors above T_c: effect of strong inelastic scattering*, M. L. Horbach, F. L. J. Vos, and W. van Saarloos, Physical Review B49, 3539 (1994) [Chapter 3].
- *Simple method for calculating the speed of sound in tight-binding models: Application to the Su-Schrieffer-Heeger model*, F. L. J. Vos, D. P. Aalberts, and W. van Saarloos, Physical Review B53, R5986 (1996) [Chapter 4].
- *Su-Schrieffer-Heeger model applied to chains of finite length*, F. L. J. Vos, D. P. Aalberts, and W. van Saarloos, Physical Review B53, 14922 (1996) [Chapter 4].
- *Towards understanding the ultra-fast dynamics of rhodopsin*, D. P. Aalberts, F. L. J. Vos, and W. van Saarloos, Pure & Appl. Chem., 69, 2099 (1997) [Chapter 5].

Curriculum Vitæ

Ik ben op 18 maart 1965 geboren in Amsterdam. Van 1977 tot 1982 bezocht ik de Christelijke MAVO te Noordwijk. Daarna volgde ik Middelbaar Laboratorium Onderwijs (MLO) aan de Laboratoriumschool Rijnland in Leiderdorp, waar vooral de bibliotheek een grote bron van inspiratie voor mij vormde. Na het afleggen van een Colloquium Doctum aan de Leidse Universiteit in april 1986, werd ik toegelaten tot de propædeuse van de studie Natuurkunde. Omdat ik eerst nog mijn militaire dienstplicht moest vervullen, kon ik pas in januari 1988 daadwerkelijk aan de propædeuse beginnen. Het propædeutisch examen behaalde ik in augustus 1989. Het afstudeeronderzoek vond plaats op het Instituut-Lorentz voor Theoretische Natuurkunde, in de werkgroep Gecondenseerde Materie bij prof. dr. ir. W. van Saarloos. De titel van mijn afstudeerscriptie luidde *On the existence of oscillatory pulse solutions in the complex Ginzburg-Landau equation.* In juni 1992 legde ik het doctoraal examen af.

In oktober 1992 trad ik in dienst van de stichting FOM (Fundamenteel Onderzoek der Materie) om als Onderzoeker in Opleiding promotieonderzoek te verrichten bij prof. dr. ir. W. van Saarloos. De belangrijkste resultaten van het onderzoek zijn beschreven in dit proefschrift. Een deel van het onderzoek is uitgevoerd in samenwerking met dr. M. L. Horbach en prof. dr. D. P. Aalberts. Mijn onderwijstaak bestond uit het geven van werkcolleges bij het college Elektromagnetisme II. Ik heb mijn onderzoeksresultaten gepresenteerd op nationale en internationale conferenties en heb deelgenomen aan diverse trainingen van de stichting FOM.

Op 1 november 1996 ben ik bij CMG Telecommunications & Utilities als consultant in dienst getreden, waar ik thans als projectleider werkzaam ben bij de divisie Advanced Technology Telecom Products.

STELLINGEN

behorende bij het proefschrift

On Fermionic Correlations
In High-Temperature Superconductors
And Molecular Systems

1. Het is denkbaar dat in hoge-temperatuur supergeleiders twee onafhankelijke mechanismen verantwoordelijk zijn voor het ontstaan van supergeleiding enerzijds en de anomale eigenschappen boven de kritieke temperatuur anderzijds.

   Hoofdstuk 2 van dit proefschrift.

2. Het in dit proefschrift beschreven scenario, waarin de mate van verstrooiing van quasi-deeltjes in de supergeleidende toestand wordt onderdrukt door het openen van een kloof in het één-deeltje excitatie-spectrum, is consistent met de experimentele resultaten van metingen van de electronische soortelijke warmte coefficient.

   A. Junod et al., Physica **C152**, *495 (1988),*
   J. W. Loram et al, Phys. Rev. Lett. **71**, *1740 (1993),*
   Hoofdstuk 2 van dit proefschrift.

3. De discrepantie tussen het door De Caluwe en Verbeure verkregen resultaat voor de geluidsnelheid in het Su–Schrieffer–Heeger model en het resultaat zoals gegeven in hoofdstuk 4 van dit proefschrift, wordt door hen onjuist verklaard; de juiste verklaring is, dat in hun berekening een niet-fysische randvoorwaarde wordt opgelegd.

   J. De Caluwe en A. Verbeure, Preprint-KUL-TF-97-21

4. Het gebruik van diagrammen met een statisch energie-landschap als functie van een reactiecoordinaat geeft in veel gevallen een onjuist beeld van de dynamica van (foto)chemische processen.

5. Wanneer een geluidsbron zich bevindt onder een stolp waaruit door pompen de lucht wordt onttrokken, is die geluidsbron uiteindelijk onhoorbaar; in tegenstelling tot wat in het natuurkunde onderwijs wordt beweerd, toont dit echter niet aan dat voor de voortplanting van geluidsgolven een medium nodig is.

6. Zij $s(n)$ de functie die ieder natuurlijk getal n spiegelt in de decimale punt: $s(1) = 0.1$, $s(621271) = 0.172126$ etc. Dan is m.b.v. de genererende functie

$$g(x, q) = \sum_{n=0}^{\infty} x^{s(n)} q^n$$

eenvoudig te bewijzen dat

$$\sum_{n=1}^{\infty} \frac{s(n)}{n(n+1)} = \frac{10}{99} \ln(10) .$$

7. Bij de beweging van een ronde schijf op een horizontaal oppervlak zijn de rotatie en translatie door de wrijving zodanig gekoppeld dat beide bewegingen, onafhankelijk van hun beginsnelheden, altijd gelijktijdig eindigen.

8. De volkswijsheid, dat een aangebroken fles mousserende wijn langer goed blijft als men een metalen lepel in de hals van de fles hangt, is inderdaad een volkswijsheid.

G. J. van Oldenborgh en F. L. J. Vos,
http://www-lorentz.leidenuniv.nl/papers/spoon.pdf,
De Volkskrant, 5 oktober 1995.

9. De slogan *Sta even stil bij het werk aan de weg* schept zeer vaak te hoge verwachtingen.

10. *Koersen op Kwaliteit* is niet mogelijk wanneer het aan voldoende voortstuwing ontbreekt.

Leiden, 2 april 1998,

F. L. J. Vos.